Macromolecular Bioscience
www.mbs-journal.de

Development of a Piezoelectric PVDF-TrFE Fibrous Scaffold to Guide Cell Adhesion, Proliferation, and Alignment

Jacob A. Orkwis, Ann K. Wolf, Syed M. Shahid, Corinne Smith, Leyla Esfandiari, and Greg M. Harris**

Severe peripheral nervous system injuries currently hold limited therapeutic solutions. Existing clinical techniques such as autografts, allografts, and newer nerve guidance conduits have shown variable outcomes in functional recovery, adverse immune responses, and in some cases low or minimal availability. This can be attributed in part to the lack of chemical, physical, and electrical cues directing both nerve guidance and regeneration. To address this pressing clinical issue, electrospun nanofibers and microfibers composed of piezoelectric polyvinylidene flouride-triflouroethylene (PVDF-TrFE) have been introduced as an alternative template for tissue engineered biomaterials, specifically as it pertains to their relevance in soft tissue and nerve repair. Here, biocompatible scaffolds of PVDF-TrFE are fabricated and their ability to generate an electrical response to mechanical deformations and produce a suitable regenerative microenvironment is examined. It is determined that 20% (w/v) PVDF-TrFE in (6:4) dimethyl formamide (DMF):acetone solvent maintains a desirable piezoelectric coefficient and the proper physical and electrical characteristics for tissue regeneration. Further, it is concluded that scaffolds of varying thickness promoted the adhesion and alignment of Schwann cells and fibroblasts. This work offers a prelude to further advancements in nanofibrous technology and a promising outlook for alternative, autologous remedies to peripheral nerve damage.

1. Introduction

Peripheral nervous system (PNS) damage manifests in over 67 000 injured Americans annually,[1] is frequently onset by conditions such as diabetes, HIV, and cancer,[2] and disproportionately affects elderly patients.[3] The PNS possesses an inherent regenerative capacity which ensures the repair of minor contusions with limited medical intervention. However, in Grade III and IV injuries, wherein the innermost endoneurial tissue in the PNS surrounding the nerve is transected, recovery is often limited and advanced surgical procedures are necessitated.[4] Neurorrhaphies are typically capable of repairing transections of shorter length yet lack the ability to fully rejoin nerve ends without inflammatory scarring or limited functional recovery.[5] For longer, more traumatic, injury gaps, nonsutured applications such as nerve conduits serve as mechanical guides for regenerative directionality while possessing interchangeable structural chemistry and a capacity for bioactive additives.[6] Nerve autografts, and in some cases allografts, are regarded as the consensus "gold standard" treatment for traumatic injury, but are hindered by availability of donor sites, risk of innervation, and more serious conditions such as neuroma.[7] Such limitations impart a demand for more personalized treatments. As tissue engineering techniques develop, specifically for neural engineering, researchers are increasingly focused on finding autologous approaches to either enhance, or replace, current remedies.

Electrospun nanofibrous polymers such as poly(ε-caprolactone) (PCL) and polyvinylidene fluoride (PVDF) are becoming increasingly relevant for tissue engineering applications. Nanofibrous scaffolds can be developed to mimic the structure of extracellular matrix (ECM) and are highly tunable to promote desired cell responses.[8] Polyvinylidene fluoride-triflouroethylene (PVDF-TrFE) copolymer exhibits a piezoelectric capacity, wherein electrical current are produced in response to mechanical deformations, mimicking important signaling events and in turn holds potential to induce regenerative phenotypes in certain cells.[9] Additionally, physical

J. A. Orkwis, C. Smith, Prof. G. M. Harris
Department of Chemical and Environmental Engineering
University of Cincinnati
Cincinnati, OH 45221, USA
E-mail: gregory.harris@uc.edu
A. K. Wolf, S.M. Shahid, Prof. L. Esfandiari
Department of Electrical Engineering and Computer Science
University of Cincinnati
Cincinnati, OH 45221, USA
E-mail: Leyla.Esfandiari@uc.edu
Prof. L. Esfandiari, Prof. G. M. Harris
Department of Biomedical Engineering
University of Cincinnati
Cincinnati, OH 45221, USA
Prof. G. M. Harris
Neuroscience Graduate Program
University of Cincinnati College of Medicine
Cincinnati, OH 45267, USA
The ORCID identification number(s) for the author(s) of this article can be found under https://doi.org/10.1002/mabi.202000197.

DOI: 10.1002/mabi.202000197

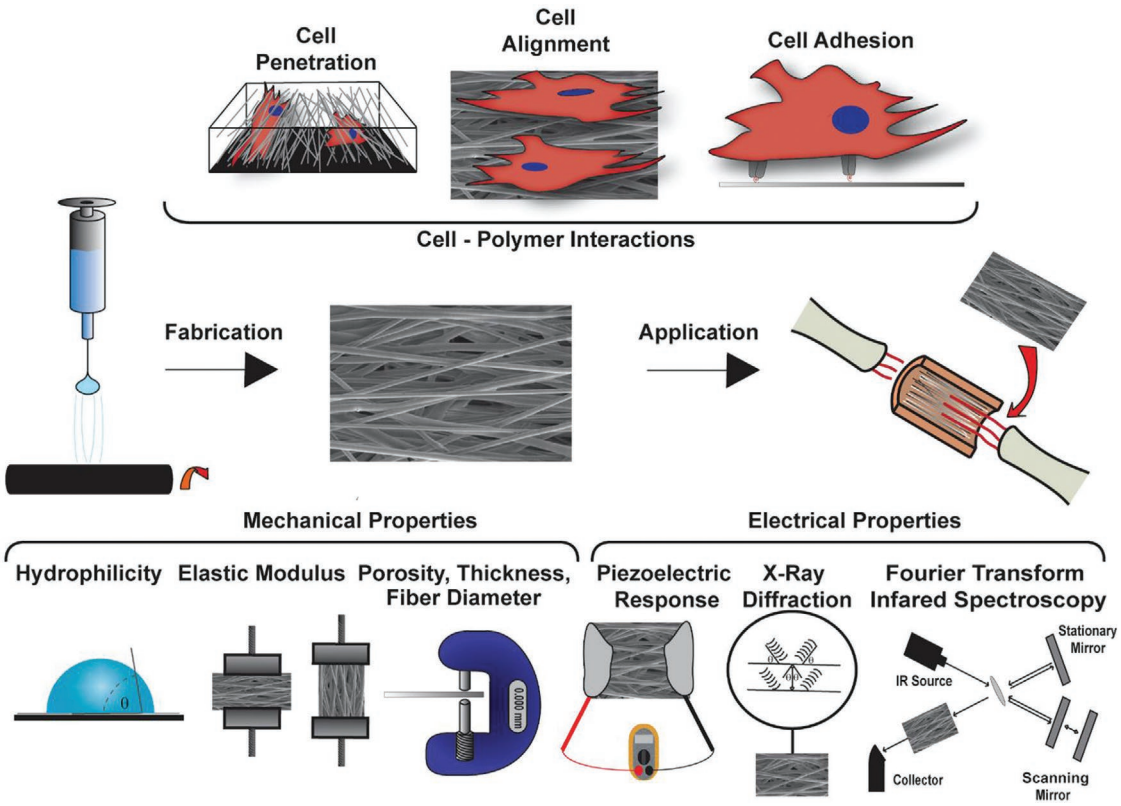

Figure 1. Schematic detailing the characterizations performed on electrospun PVDF-TrFE scaffolds. Characterizations are delineated as mechanical properties (bottom left), electrical properties (bottom right), and cellular response to scaffolds (top).

parameters of the nanofibrous scaffolds such as porosity, elastic modulus, fiber diameter, hydrophilicity, and alignment can be tailored to meet specific tissue demands.[10] The resulting scaffolds with tunable physical, chemical, and electrical properties offer distinct advantages over other nanofibrous materials and regenerative devices. Primarily, electrical impulses can be administered to cells and thereby remodel tissue without the need for external power sources.[11] Moreover, PVDF-TrFE offers a straightforward template for biomaterials that can be enhanced with bioactive components, combined with preexisting technologies, or developed as independent clinical solutions for multiple types of tissue injury.

Relatively little work has been done to characterize PVDF-TrFE in current therapeutics thus far, but preliminary studies have begun to catalogue the response of cells and molecules to the polymer. In vitro models have been shown to promote osteogenic differentiation of human mesenchymal cells and early mineralization of the corresponding ECM,[12] differentiation of human neural stem/progenitor cells and neuron mimicking PC-12 cells,[13–15] neuron and neurite extension of dorsal root ganglia,[16] and alignment and proliferation of Schwann cells and fibroblasts.[16,17] Though scarce in total, in vivo models have utilized PVDF-TrFE as nerve conduits to enhance regeneration of axons, ancillary cells, and neurotrophic factors such as astrocyte processes and blood vessels.[18,19]

The tunable physical, chemical, and electrical properties of PVDF-TrFE make fabricated scaffolds an ideal template for PNS biomaterials. Specifically, the piezoelectric capacity of the fibers complements the distinct electrical environment characterizing the nervous system. Though researchers have studied the phenomenon in multiple biological structures such as keratin,[20] collagen,[21] and bone,[22] and a general understanding exists regarding the positive effect of piezoelectricity on cell behavior, there is an extensive lack of information regarding the broader correlation between PVDF-TrFE properties and tissue repair. By contrast, the role of individual cells in PNS repair is well established. For instance, Schwann cells dedifferentiate into a regenerative phenotype that secretes extracellular matrix proteins and subsequently provides a template for axon growth.[23–27] Likewise, fibroblasts have been identified as crucial supportive cells that promote the alignment and migration of Schwann cells while simultaneously depositing additional ECM proteins and neurotrophic factors.[19,26] Therefore, this work aims to create tunable PVDF-TrFE scaffolds with extensive characterization of the parameters beneficial to a regenerative neurotrophic environment. Uniquely, Schwann cells and fibroblast cells were used to determine the morphological cell response to varied electrospinning parameters through quantified measurements including cell alignment, elongation, and viability. A thorough examination of the electrospun polymers will provide a mechanistic view into their use as practical supplements and alternatives to current clinical procedures for peripheral nerve damage (**Figure 1**).

2. Results and Discussion

2.1. Characterization of Fiber Morphology, Tensile Strength, and Hydrophobicity

To first establish the efficacy of PVDF-TrFE scaffolds as suitable tissue engineering substrates, the physical characteristics of fiber alignment, fiber diameter, scaffold porosity, scaffold thickness, surface hydrophilicity, and tensile strength were examined. Scaffolds were created by electrospinning 20% (w/v) PVDF-TrFE in (6:4) DMF:acetone solution for 1, 2, or 3 h. Resultant fibers showed uniform morphology and a clear alignment for aligned versions of the scaffold (**Figure 2**A, Figure S1, Supporting Information). All scaffolds, regardless of spin time, exhibited a mean fiber diameter of 1.0046 ± 0.038 µm, which is notably less than scaffolds previously fabricated under similar conditions (2000 rpm) with an average fiber diameter of 1.56 ± 0.60 µm. [28] Small fiber diameters across multiple electrospinning times suggest our fabrication technique can potentially produce both enhanced piezoelectricity and preferential

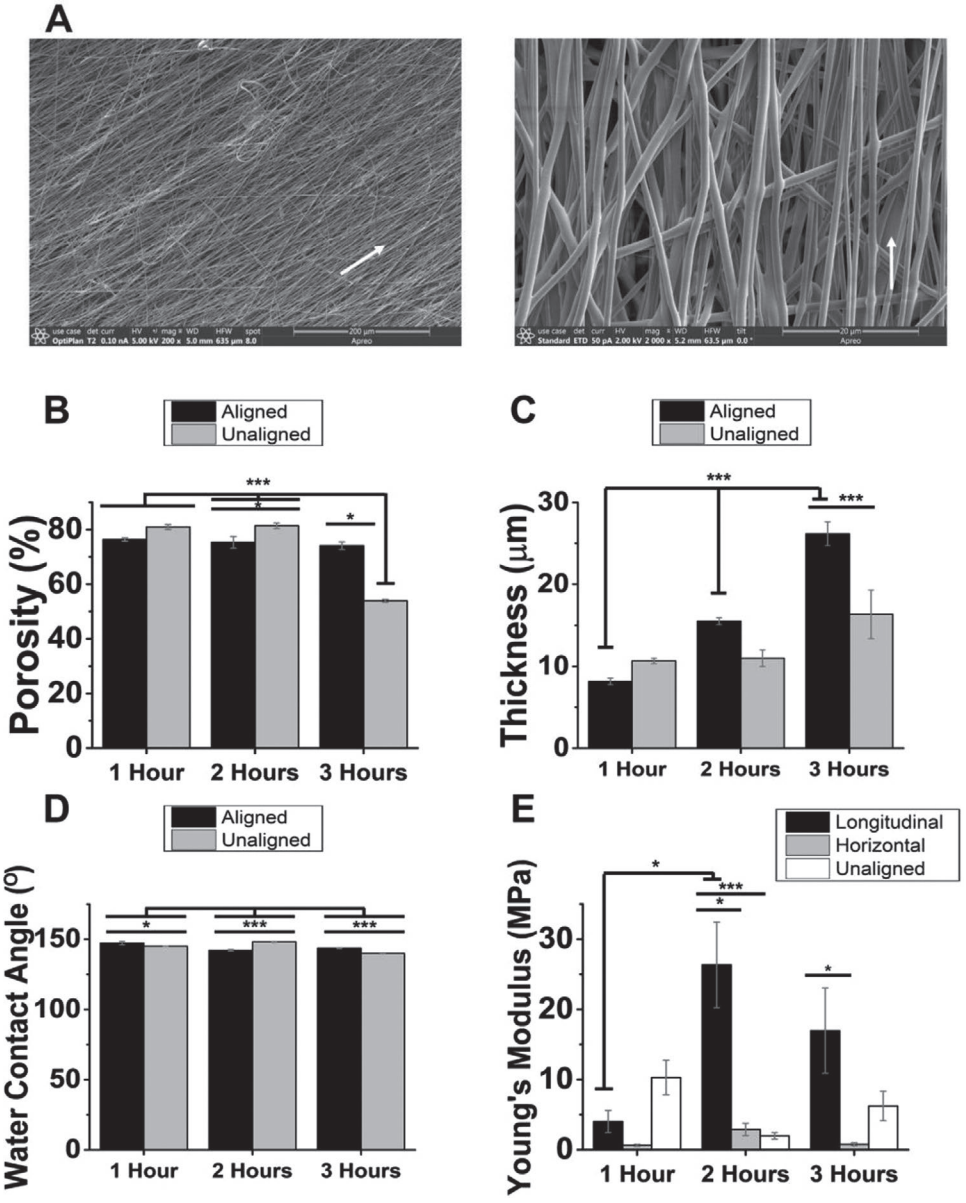

Figure 2. Mechanical characterization of PVDF-TrFE scaffolds. A) Representative SEM images of PVDF-TrFE scaffolds spun for 2 h at 200× (left) and 2000× (right) magnification showing uniform alignment. White arrow indicates intended direction of alignment. Scale bar = 200 µm (left) and 20 µm (right). B) Porosity calculations for both aligned and unaligned PVDF-TrFE scaffolds, $n = 6$ unique trials per condition. C) Thickness measurements for both aligned and unaligned PVDF-TrFE scaffolds, $n = 3$ unique trials per condition. D) Water contact angle for both aligned and unaligned PVDF-TrFE scaffolds, $n = 5$ unique trials. E) Young's moduli of PVDF-TrFE scaffolds tested both longitudinally and perpendicular (relative to alignment) for aligned fibers and without directionality for unaligned fibers, $n = 3$ unique trials per condition. All data recorded for scaffold fabrication times of 1, 2, and 3 h. Data are reported as mean ± SEM. $^{*}p \leq 0.05$; $^{**}p \leq 0.005$; $^{***}p \leq 0.0005$.

cell-scaffold interactions. First, a negative logarithmic relationship between fiber diameter and piezoelectric constants[29] ensures that cells cultured on smaller electrospun fibers tend to respond with higher rates of proliferation and lower cell spreading.[30,31] In the context of PNS regeneration, it is further encouraging that our fiber diameters were not excessively small (less than 1 μm) . For instance, neurite length and cell area tend to extend or spread more favorably on micron-sized fibers as opposed to nanosized fibers, a possible consequence of the nanosized fiber interaction with cell integrins.[13,30] Therefore, these fiber diameters may prove ideal both from a purely physical perspective and in the context of piezoelectric output.

All scaffold conditions exhibited estimated porosity values greater than 70%, except unaligned fibers spun for 3 h (Figure 2B), far exceeding previously reported values (54%), potentially as a consequence of using a highly volatile solvent.[32] As expected, aligned scaffolds were less porous than unaligned scaffolds (Figure 2B). Interestingly, for aligned fibers, longer spin times increased scaffold thickness but did not significantly affect the estimated porosity (Figure 2B,C, Table S1A,B, Supporting Information). The porosity of biomaterials incurs a multifaceted effect on tissue regeneration; sufficient porosity must be maintained to allow cells to adequately penetrate the surface, produce 3D cultures with proper nutrient diffusion and adequate revascularization, prevent excessive cell-to-cell contact that could limit growth and result in apoptosis,[12] and elongate cells along aligned axis, thereby preserving tunable directionality.[33] By contrast, the importance of scaffold thickness is less elucidated. In electrospun PCL nanofibrous scaffolds, thicker scaffolds promoted proliferation of carcinoma stem cells, epithelial kidney cells, ovary cells, and mesenchymal stem cells,[34] but little is known regarding PVDF-TrFE. This distinction offers a unique advantage for researchers; scaffold thickness can be increased to enhance the clinical applicability of PVDF-TrFE scaffolds to other tissue while sufficient porosity is maintained.

Water contact angles were analyzed on the fiber surface as another important regenerative marker (Figure S2, Supporting Information). Cell proliferation, adhesion, and viability are all enhanced by hydrophilic substrates,[35] yet electrospun scaffolds are typically hydrophobic.[36] We observed that 2 h aligned scaffolds (142.12° ± 0.71°) were significantly more hydrophilic than either 1 (147.28° ± 0.31°) or 3 (143.63° ± 0.29°) h aligned scaffolds (Figure 2D, Table S1C, Supporting Information). It has been suggested that a more porous scaffold can produce a more hydrophilic surface.[37] However, 2 h aligned scaffolds (75.36 ± 2.11%) were less porous than 2 h unaligned scaffolds (81.40 ± 1.03%), while the aligned scaffolds were, in fact, more hydrophilic (Figure 2B,D, Table S1A,C, Supporting Information). In contrast, the opposite was true for 1 and 3 h aligned scaffolds compared to unaligned scaffolds (Figure 2B,D, Table S1A,C, Supporting Information).

The absence of a holistic trend arising between thickness, porosity, and hydrophilicity suggests that one favorable physical characteristic for tissue engineering does not necessarily exist at the expense of other favorable characteristics. Here we have shown that thicker scaffolds can be developed that maintain consistent porosity without affecting surface hydrophilicity. Nevertheless, all scaffolds were still substantially more hydrophobic than previously reported values, with contact angles greater than 130°.[38] As a relatively simple solution, oxygen plasma treatment has been used to alter the surface chemistry of fibers to enhance hydrophilicity[35] in addition to more elegant solutions involving the modification and patterning of the surface chemistry of material.[39] Ideally, fiber diameters and scaffold porosity can be maintained in fabrication while thickness and hydrophilicity can be altered to benefit individual cells and the piezoelectric output.

Mechanical testing of elastic moduli for the scaffolds displayed significant variability (Figure 2E, Table S1D, Supporting Information). Increased spin times (3 h) produced aligned fibers with a greater longitudinal tensile strength with fibers (16.96 ± 6.06 MPa) than shown perpendicular to the aligned fibers (0.78 ± 0.23 MPa) or compared to unaligned fibers (6.24 ± 2.10 MPa) . Though previous tensile measurements are scarce for PVDF-TrFE scaffolds, Lee and Arinzeh demonstrated similar results for their unaligned polymers, but significantly greater moduli for aligned polymers,[13] reporting moduli values of 5.88 ± 2.89 and 225.28 ± 53.63 MPa for unaligned and aligned scaffolds, respectively. As mentioned, their unaligned scaffolds possessed significantly higher elastic modulus, but with a high relative proportion of error (49.1% and 23.8% for unaligned and aligned, respectively). As a potential means for greater control, Banisadi et al. were able to effectively increase the tensile strength of PVDF-TrFE scaffolds by raising the annealing temperature. However, the treatment did not mitigate the relatively high proportional error.[40]

In some cases, our scaffolds were similar in longitudinal tensile strength to a mean elastic modulus of 13.79 ± 5.48 MPa in rat sciatic nerves.[41] All three conditions displayed unique relative magnitudes for each fiber orientation, where unaligned fibers were the strongest for 1 h (10.30 ± 2.45 MPa), longitudinally aligned fibers (26.33 ± 6.09 MPa) were the strongest for 2 h but with stronger perpendicular tested fibers (2.89 ± 0.89 MPa) than unaligned (1.98 ± 0.47 MPa) , and longitudinally aligned fibers (16.96 ± 6.06 MPa) strongest for 3 h (Figure 2E; Table S1D and Figure S3, Supporting Information). Stachewicz et al. have also previously demonstrated an inverse, negative logarithmic relationship between fiber diameter and polymer elasticity on a nanolevel.[42] Likewise, Amoroso et al. demonstrated flexibility in electrospun scaffold moduli by altering porosity and introducing specific microstructural alterations.[43] Due to the anisotropic nature of electrospun PVDF-TrFE fibers as more characteristic of native tissue, care must be taken to limit rheological variability in production.

However, the broad range of tensile strength capable of being achieved by the scaffolds offers many advantages. Researchers have demonstrated control over cell proliferation, adhesion, spreading, and differentiation by manipulating moduli in electrospun PCL and silk fibers.[17,44] Further, regenerative environments are often reliant on tissue stiffness to alter the phenotype of cells.[45–48] For instance, it has been previously demonstrated that polydimethylsiloxane (PDMS) substrates can be fabricated over a broad range of physiologically relevant Young's Moduli to promote durotaxis and phenotype change of Schwann cells.[24,41] It was also shown that an intermediate substrate stiffness promotes the proliferation of

Schwann cells and expression of the dedifferentiated Schwann cell marker c-jun.[24] In broader applications, the extracellular matrix has received a renewed interest in relation to rheological mediation of cell behavior during development, disease, and regeneration. For instance, ECM stiffening has been directly linked to tumor progression for various cancers.[49] Toward this, fibroblasts are known to preferentially migrate toward stiffer surfaces and experience distinct morphological changes in area and shape as substrate moduli change.[50] By contrast, increased substrate stiffness appears to inhibit neurite extension, indicative of the softer matrices assembled by healthy tissue.[51,52] In addition the density, and in effect stiffness, of ECM has a high impact as it can sequester and release cell-secreted factors such as fibroblast growth factor (FGF) to mediate a response during regeneration.[49]

Ultimately, while it is desirable to fabricate stronger scaffolds, we have emphasized the elastic diversity of electrospun PVDF-TrFE. For clinical applications, scaffolds of variable elasticity may eventually be developed to match the stiffness of regenerating physiological tissue. An improvement to both the electrical properties and elastic moduli could be obtained by the addition of carbon nanotubes, which have been used to increase tensile strength of PVDF mats while simultaneously increasing piezoelectric coefficients.[53] Jeong et al. also demonstrated relatively consistent PVDF-TrFE scaffold moduli of 3.5 ± 0.3, 3.6 ± 0.2, 4.0 ± 0.3, 4.5 ± 0.5, and 5.2 ± 0.4 MPa using polyhedral oligomeric silsesquioxane–epigallocatechin gallate conjugates.[54] However, unlike scaffold thickness and hydrophilicity, elastic moduli are likely to be more susceptible to changes in fiber diameter and scaffold porosity.

2.2. Crystallinity of Scaffolds

PVDF-TrFE is a semi-crystalline polymorphic polymer that exists in five phases, the most prominent of which being α, β and γ.[55] After examining the physical characteristics of the scaffolds, the relative proportion of β phase configuration was examined by Fourier Transform Infrared Spectroscopy (FTIR) and used as a test for piezoelectric capacity. The FTIR spectra showed characteristic bands of the β phase in all samples, including 470, 840, 880, 1285, and 1399 cm^{-1}.[22,45] All samples also presented bands at 408 and 510 cm^{-1}, indicative of the α phase (**Figure 3**A).[45] The β phase percentage was calculated for all electrospun scaffolds and showed no significant differences between spin times, where 1, 2, and 3 h spun scaffolds were 88.49%, 87.44%, and 88.37% configured in β phase, respectively. The β configuration, which is reflective of the *trans-(TTTT)* planar conformation, exhibits the highest dipole moment of the three phases, primarily resulting from the polarity of unidirectional carbon-fluorine bonds.[56] While the standard PVDF polymer typically requires electrical poling to induce the piezoelectric β phase, the addition of the TrFE monomer forces PVDF into the all *trans-(TTTT)* conformation.[54] FTIR results emphatically reflected the prevalence of β phase throughout all fabrication conditions and the piezoelectric capacity of all fibrous scaffolds.

Inherent overlap present in FTIR between α phase and β phase necessitated use of X-Ray diffraction (XRD) to further analyze the chemical composition of scaffolds.[22] XRD spectra for unprocessed PVDF-TrFE powder and all electrospun fibers exhibited similar patterns (Figure 3B). The β phase can be identified from its characteristic peak around $2\theta = 20°$ in the (1 1 0) and (2 0 0) planes. The presence of this phase was reflected by a peak produced at $2\theta = 19.8°$ corresponding to the (1 1 0) and (2 0 0) planes of the β-phase crystal structure.[55,57] Additionally, the α phase, which has peaks around 17.66° and 18.3° corresponding to the (1 0 0), (0 2 0) and (1 1 0) planes, was reflected in the powder by a peak at $2\theta = 18.3°$. The primary peak of the electrospun PVDF-TrFE fibers was located at $2\theta = 19.9°$ (also corresponding to the 200/110 reflection) and lacking the peak at 18.3°. Though more difficult to quantify than FTIR, XRD spectra further confirmed the ideal crystalline structure attained in our scaffolds and the capacity for piezoelectricity.

2.3. Piezoelectric Output of Scaffold

After examining the physical characteristics and crystallinity of the PVDF-TrFE scaffolds, piezoelectric output was qualitatively analyzed by measuring the induced electrical current in response to mechanical stretching of the fibers (Figure 3C). As external stress was applied to the scaffolds, an impulse response was produced in the form of an increase in magnitude of current (Figure 3D). With the exception of inherent noise from the system, no signal was created without applied stress to the piezoelectric fibrous scaffold. When the scaffolds were stretched upward a positive current was induced, which became negative when the pressure was released (Figure 3D). The maximum current output was 1.75 nA, while the absolute value of the average of all peaks was 0.76 nA. While prior work observed a maximum induced current of 40 nA for fibrous scaffolds, the vast difference is likely attributable to our smaller scaffold thickness (where a thicker scaffold produces higher currents).[58] A piezoelectric response of the PVDF-TrFE scaffolds may be able to provide a significant electric stimulation due to the deformations caused by cell attachment and migration, where cells have notably been shown to contract their matrices by 1 to 3 μm in vitro,[24] and the general locomotion of tissue and adjacent biological structures. To artificially promote the piezoelectric effect, alternative techniques such as noninvasive ultrasound can be used to incur polarization and subsequent differentiation of cells.[59] Further, scaffolds were confirmed to have high resistivity when no stress was applied (Figure S4, Supporting Information) and produced a maximum current of 6 pA, showing no significant difference in output relative to control.

In short, we have utilized a rudimentary method establishing that an electric current is induced in scaffolds in response to mechanical deformation. While aligned fibrous scaffolds made of nonpiezoelectric polymers such as PCL are capable of directing Schwann cell elongation and encouraging cell maturation,[60] the piezoelectricity of PVDF-TrFE exhibits a unique potential to provide additional stimulatory cues for cells. For instance, Schwann cells stimulated by a 50 mV mm^{-1} electric field showed increased neurite outgrowth and increased alignment in the direction of the electric field, as well as increased

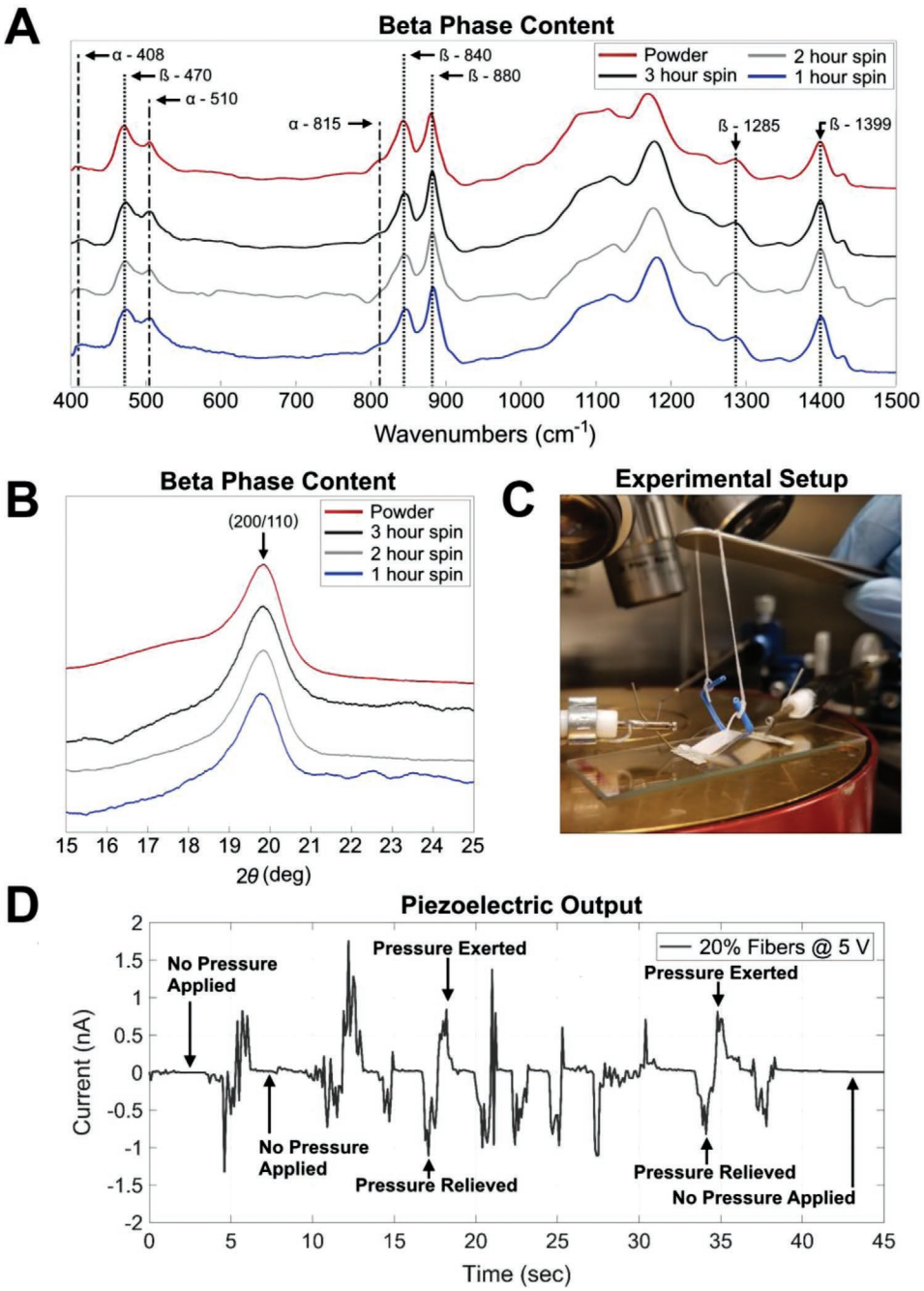

Figure 3. Characterization of the piezoelectric property of PVDF-TrFE scaffolds. A) Fourier transform infrared spectroscopy performed on PVDF-TrFE powder and scaffolds fabricated for 1, 2, and 3 h. Dashed lines correspond to peaks characteristic of either α or β phase, as labeled. B) X-ray diffraction performed on PVDF-TrFE powder and scaffolds fabricated for 1, 2, and 3 h. A peak at 19.9° (2θ) indicates ample β phase content. C) Image depicting experimental setup for piezoelectric output measurements. Conductive silver paint coated on each end of scaffold and attached to voltmeter was used to measure the current resulting from an applied mechanical deformation as shown. D) Current output from piezoelectric response in 2 h aligned scaffolds. Dashed lines emphasize cyclic amplitudes interspersed with plateaued signals, showing electrical activity immediately post deformation and at rest, respectively.

release of nerve growth factor post-stimulation.[61] Moving forward, quantitative investigation of the piezoelectric response induced by electrospun scaffolds can be analyzed in conjunction with ultrasound stimulation and biological stimuli for translation of the platform.

2.4. Cell Adhesion and Integration with Scaffold

To examine the biocompatibility of PVDF-TrFE scaffolds, cells with or without serum were measured for adhesion to scaffolds. Additionally, scaffolds were either coated with laminin

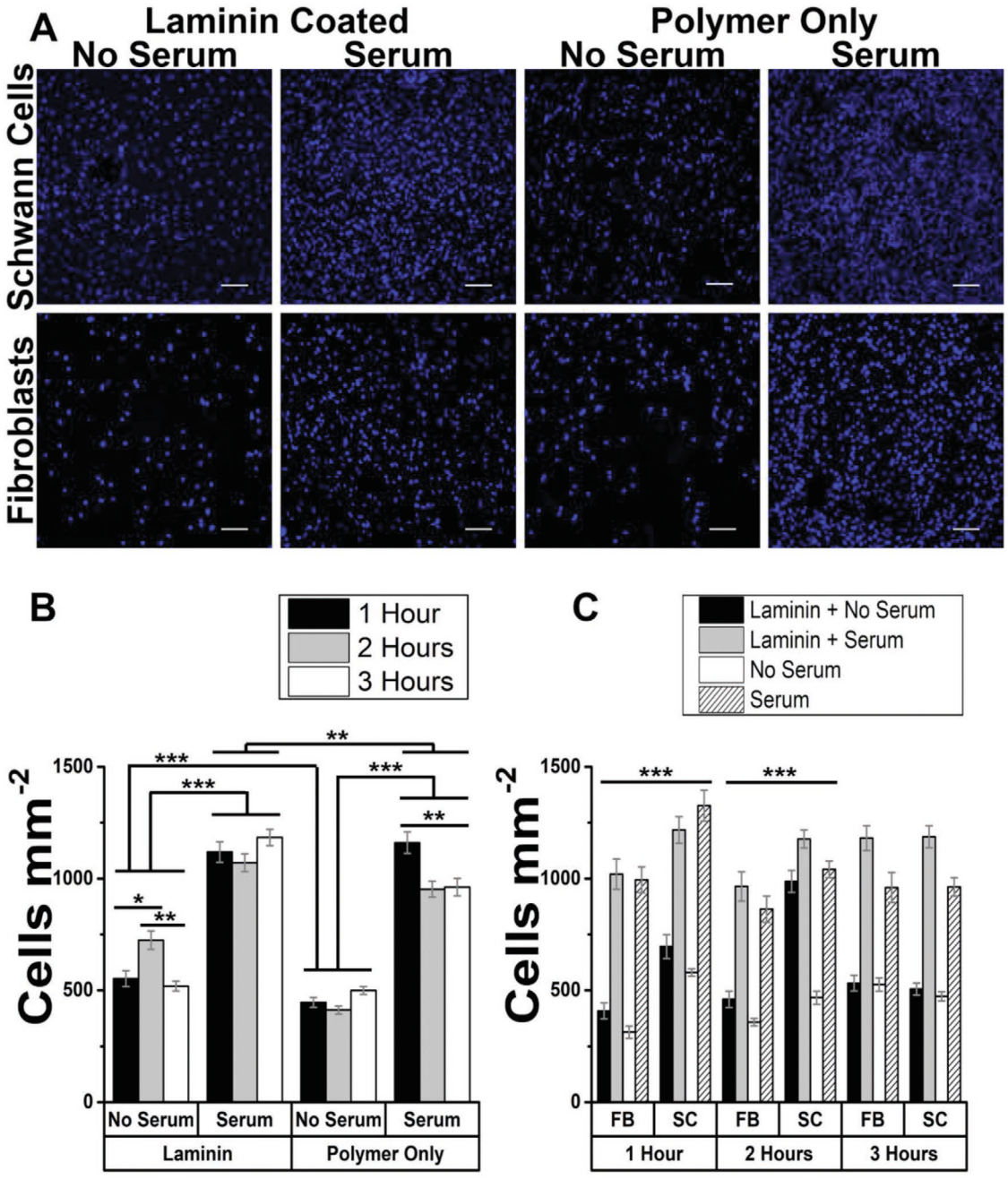

Figure 4. Cell adhesion on aligned PVDF-TrFE scaffolds was promoted by both laminin coatings and either fetal bovine serum (for Schwann cells) or bovine calf serum (for fibroblasts). A) Representative images showing adherent cell nuclei supplemented with either serum or no serum cultured on PVDF-TrFE scaffolds with (left) or without (right) laminin coatings. Images shown for cells on 1 h aligned scaffolds. Scale bars = 100 µm. B) Adherent cells detected for each condition on scaffolds fabricated for 1, 2, and 3 h. C) Individual Schwann cells and fibroblasts detected for each condition on scaffolds fabricated for 1, 2, and 3 h. A–C) $n = 3$ unique trials per condition seeded at 750 cells mm^{-2}, with 15 images captured per trial after 24 h of culture. Data are reported as mean ± SEM. $^{*}p \leq 0.05$; $^{**}p \leq 0.005$; $^{***}p \leq 0.0005$.

or left uncoated. Changes in electrospinning time resulted in significantly different adhesion properties, but no clear trend was evident (**Figure 4**A,B, Figure S5, Supporting Information). Though intermediate spin times (2 h) tended to produce more favorable physical characteristics of thickness, hydrophilicity, and tensile strength (Figure 2C–E), greater β phase configuration, and piezoelectric output (Figure 3A,B), there was no clear increase in adhesion relative to other spin times. While all conditions exhibited a capacity for sustainable cell growth, there was immense variability regarding the combinatorial effect between supplemented proteins and electrospinning times. In cultures deplete of proteins (no serum, no laminin) and cultures with both supplements added (serum and laminin), 3 h electrospun scaffolds significantly enhanced adhesion

(Figure 4B,C; Figure S5 and Table S2, Supporting Information). In cultures with only one supplement provided (either serum or laminin, but not both), both 1 and 2 h spun scaffolds significantly enhanced adhesion relative to 3 h spun scaffolds (Figure 4B,C; Table S2 and Figure S5, Supporting Information). And thus, while it could not be established that specific fabrication conditions, or physical and electrical characteristics, were more important to cell viability than others, it is notable that cells were capable of adhering to all scaffolds both with and without supplements, thereby further suppressing concerns that DMF:acetone solvent mixtures for electrospun applications deleteriously affect cells.

In both cases with or without serum, a laminin coating produced a significant increase in cell adhesion (Figure 4A,B, Table S2, Supporting Information). Laminin plays a unique role in the PNS relative to other ECM proteins as it primarily composes the basement membrane of the endoneurial tissue surrounding nerves and is responsible for Schwann cell adhesion, migration, and dedifferentiation during development and regeneration.[37,62] Though serum had a more pronounced effect on cells, laminin still significantly promoted adherence relative to other cultures (Figure 4B, Table S2, Supporting Information). The dramatic increase resulting from laminin coatings can be attributed to the aforementioned interplay amongst Schwann cells and the protein, as well as the Schwann cell's role in axon polarization and myelination.[63] As expected, Schwann cells responded to laminin with significantly more adherence than fibroblasts (Figure 4C, Table S2, Supporting Information). However, laminin coatings still promoted greater adherence in fibroblasts than cultures without serum (Figure 4C, Table S2, Supporting Information). While Schwann cells are more commonly associated with the endoneurial tissue, the prevalence of both cells in the PNS intuitively suggests the presence of laminin receptors on fibroblast cell membranes as well,[64] which is further supported by specifically detected binding proteins at 110 and 120 kDa.[65,66]

Furthermore, the proliferative capacity on both unaligned and aligned fibers for Schwann cells and fibroblasts was examined. On both scaffolds, Schwann cells and fibroblasts were capable of proliferation over 3 d (**Figure 5**A). After 72 h, cells began to reach a confluent state on the polymers, but the dimensionality of the scaffolds and the low seeding density ensured that cells did not form in a distinct uniplanar culture (Figure 5B). There were no significant differences in the proliferation of cells on unaligned fibers and aligned fibers (Figure 5C) nor between each cell, with the exception of those cultured for 72 h on unaligned polymers. Ultimately, cells were significantly more abundant with each subsequent day (Figure 5D).

Electrospun fibers can be modified to specifically promote cell proliferation in the context of wound regeneration,[30,31,34] and piezoelectric materials in particular have a unique capacity for enhancing replication of numerous cell types.[16,54,59,67] For instance, Wang et al. demonstrated that modulation of the piezoelectric effect in PVDF-TrFE nanofibers with targeted vibrations can increase the proliferation rate of fibroblasts 1.6 fold.[68] Therefore, these results in conjunction with the adhesion assay show both unaligned and aligned scaffolds are biocompatible and capable of facilitating cell proliferation.

We further analyzed cell penetration to better understand how cells integrate into the scaffold promoting contact guidance. To assess depths of penetration, scanning electron microscopy (SEM) imaging was conducted to examine cells cultured on scaffolds (**Figure 6**A) and confocal microscopy, utilizing multilevel *Z*-stack images up to 35 µm of depth, was performed to examine the corresponding cell location and morphology. Projections for cell-scaffold cultures showed that both Schwann cells and fibroblasts penetrated the entire depth of the scaffold (Figures 6B,C and 7A,B), adhering and elongating at depths of up to 30 µm in unaligned scaffolds and 20 µm in aligned scaffolds. Cell alignment was consistent throughout the scaffolds and encouragingly suggests that regenerative cues can be maintained at different thickness fabrications. Therefore, if polymer thickness can be increased while maintaining adequate physical characteristics, piezoelectric capacity, and favorable cell responses, scaffolds become increasingly more viable as translatable tissue engineering devices.[69]

Despite penetration of cells to all depths of the scaffold, cultures were primarily localized between ≈10 and 12 µm of depth, suggesting that cells predominantly grew at, or near, surface level of the scaffolds in the short time periods analyzed (Figures 6Ai and 7). Understanding that this may have been a limitation of a short culture incubation (24 h), cells were also grown for 72 h and examined with SEM. At this higher density, a more 2D-like culture emerged at or near the surface of the scaffold (Figure 6Aii). It is possible that the micron-sized fiber diameters provided a small surface area-to-volume ratio that promoted unidirectional cell elongation (consistent alignment), but decreased multidimensional cell spreading.[13,30] While cell penetration within scaffolds is crucial to tissue repair,[70] further work must focus on maintaining dimensionality throughout longer incubation periods. It is also possible to subvert this caveat by developing integrated devices, such as 3D electrospun, aligned nerve conduits, that incorporate additional material technology to affect cell phenotypes in feasible clinical applications.[16,41]

2.5. Cell Alignment on Scaffolds

Qualitatively, our fibers promoted alignment in both Schwann cells and fibroblasts (**Figure 8**A) consistent with previous work.[16,18,68] To further confirm the extent of alignment, we performed fast Fourier transformations (FFT) on F-actin labeled images to examine alignment of the cell cytoskeleton (Figure 8B,C). Full width at half-maximum values were obtained and used as quantification for cell alignment. Aligned PVDF-TrFE fibers emphatically promoted the alignment of both Schwann cells and fibroblasts relative to both unaligned PVDF-TrFE fibers and glass coverslips (Figure 8D,E, Table S3, Supporting Information). Alignment is commonly perceived as an indicator of a regenerative PNS phenotype as it is essential for cells to properly align along injury gaps and form the foundation upon which Bands of Büngner, the ECM-rich pathways responsible for directing axon regeneration, are constructed.[60,71] Though fibroblasts were significantly less aligned on unaligned fibers of longer spin time (2 and 3 h) than Schwann cells, there were no other

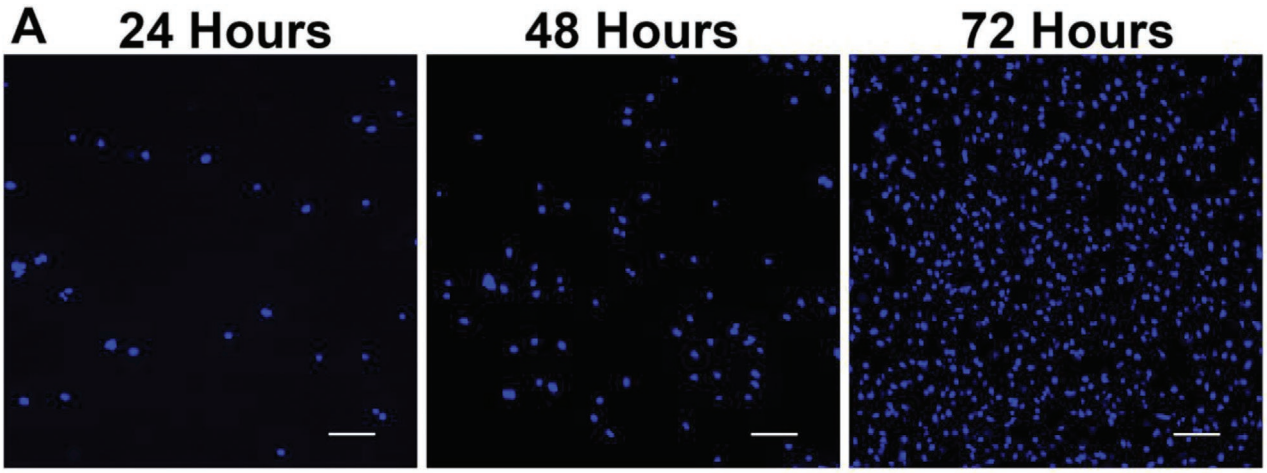

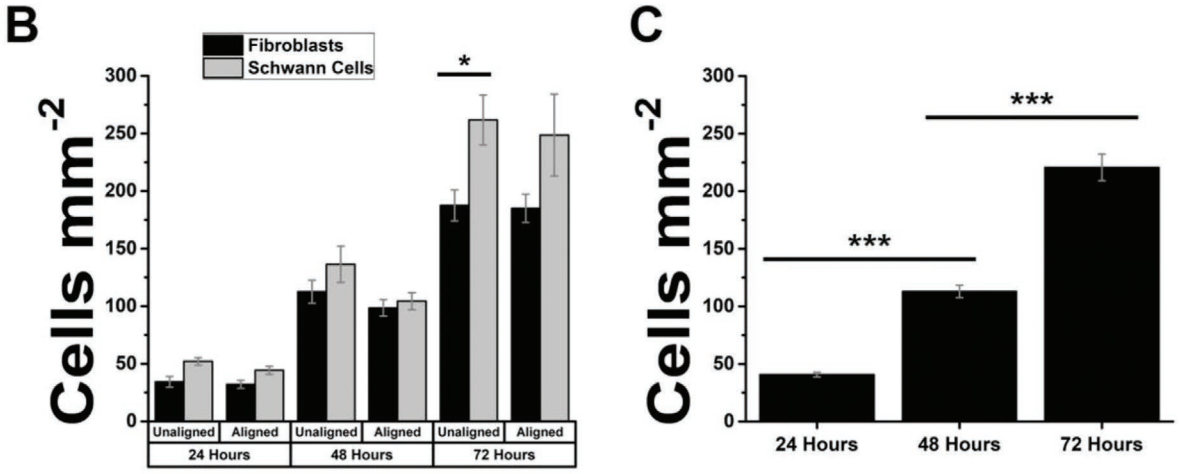

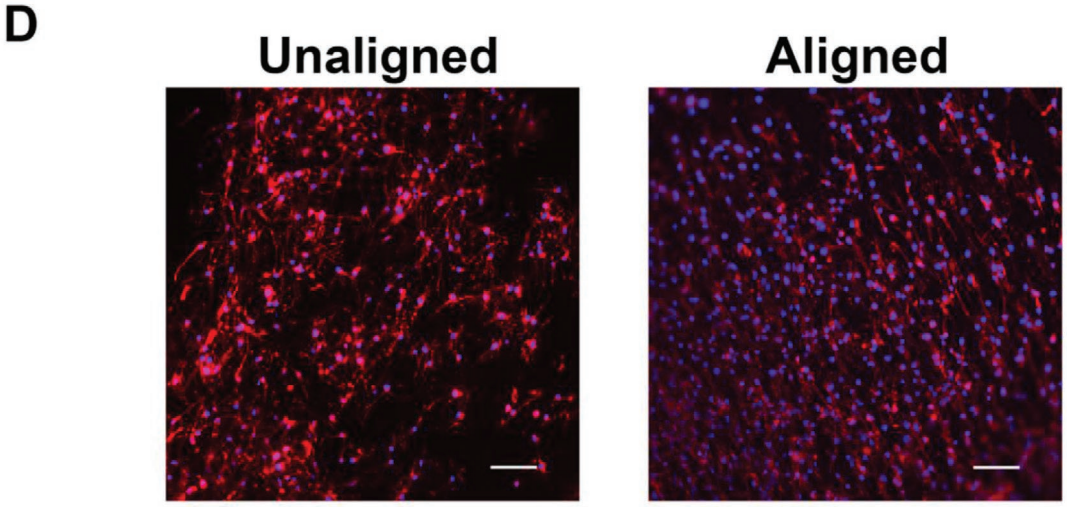

Figure 5. Schwann cells and fibroblasts proliferated on 2 h electrospun unaligned and aligned PVDF-TrFE scaffolds. A) Representative DAPI images depicting proliferation at 24, 48, and 72 h. B) Average number of fibroblasts and Schwann cells per mm^2 on unaligned and aligned polymers after 24, 48, and 72 h. $n = 3$ unique trials per condition seeded at 50 cells mm^{-2}, with 15 images captured per trial. Data are reported as mean ± SEM. $^{*}p \leq 0.05$; $^{**}p \leq 0.005$; $^{***}p \leq 0.0005$. C) Average of Schwann cell and fibroblast proliferation at each time point. D) Representative images showing alignment of cells after 72 h with rhodamine-phalloidin (red) and DAPI (blue).

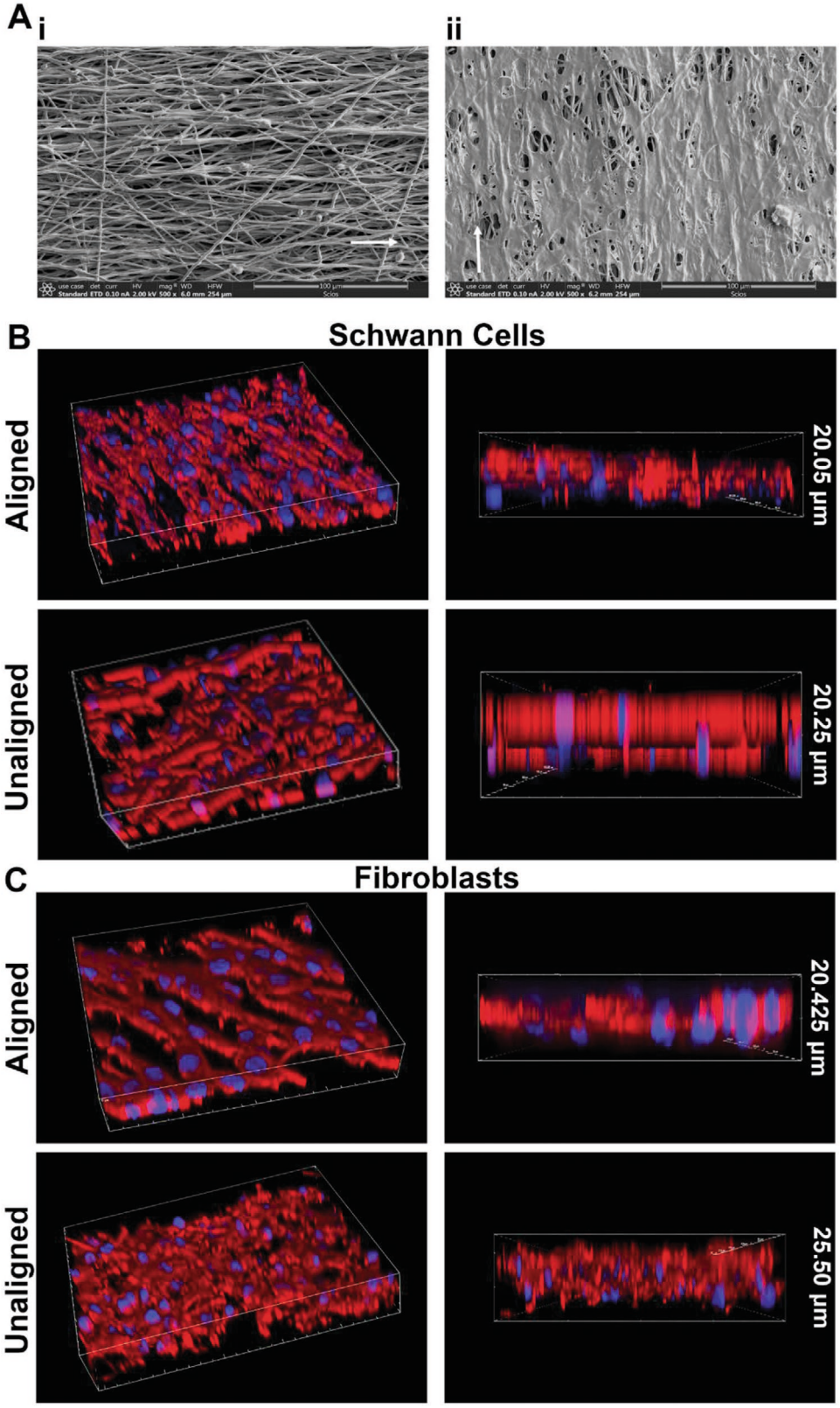

Figure 6. Cells can penetrate scaffolds, but cultures are largely uniplanar. A) Representative SEM images at 500× magnification of cells cultured on 1 h aligned scaffolds for 24 h (left) and 72 h (right) and interspersed within fibers. Scale bar = 100 µm. Representative confocal *z*-stack 3D, alpha blended projections showing B) Schwann cells and C) fibroblasts penetrating 1 h aligned and unaligned scaffolds after 24 h of culture, offset view (left) and *XZ*-plane cross section (right), $n = 3$ unique trials per condition seeded at 750 cells mm^{-2}, with two images captured per trial after 24 h of culture.

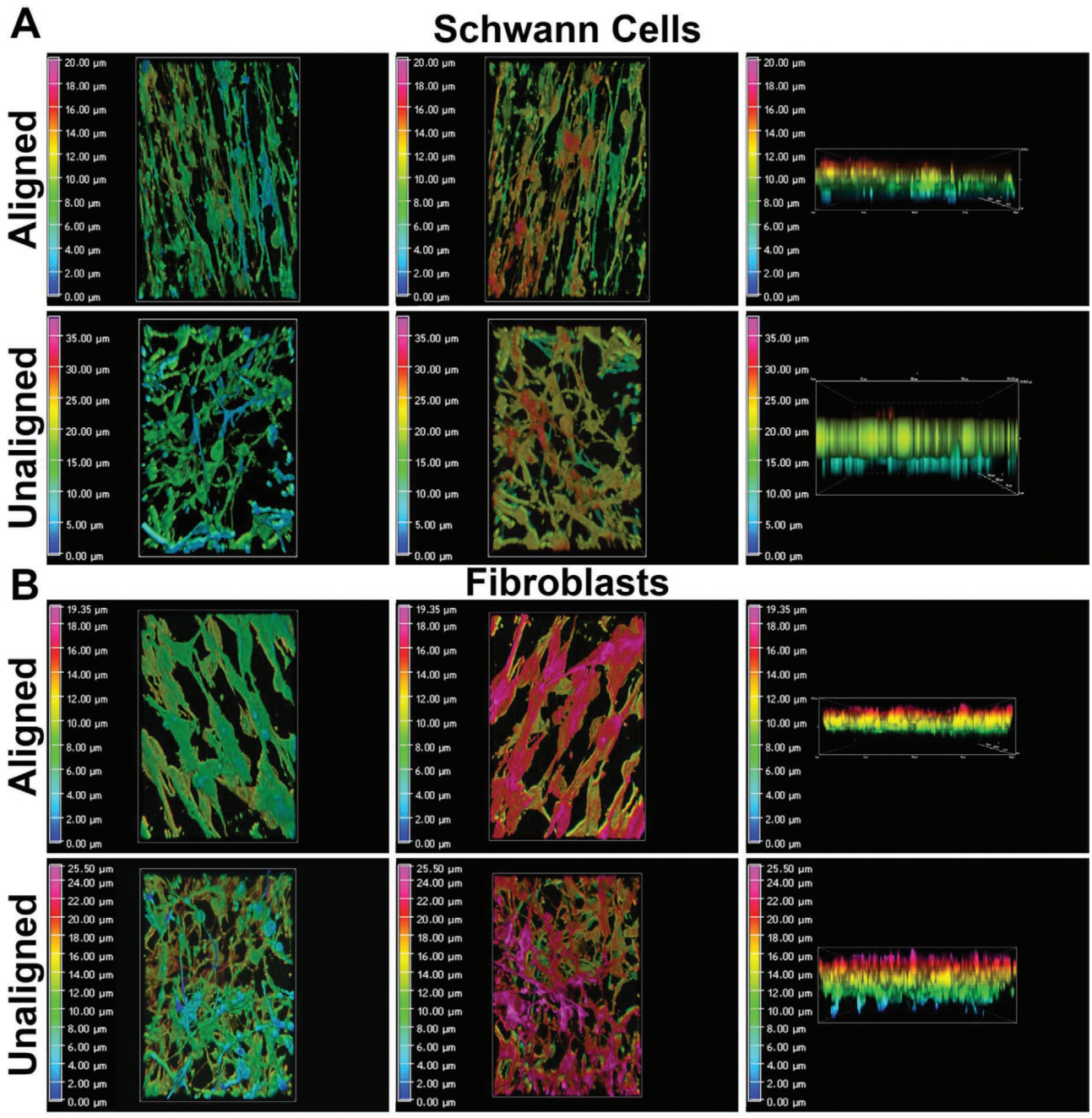

Figure 7. Representative confocal microscopy reconstructed 3D models of A) Schwann cells and B) fibroblasts seeded on aligned and unaligned PVDF-TrFE scaffolds electrospun for 1 h. Figure shows an assessment for penetration of cells into the scaffold through color coded, alpha blended depth projections as viewed from the *XY* plane (left), flipped *XY* plane (center), and cross sectional *XZ* plane (right) of the scaffolds, $n = 3$ unique trials per condition seeded at 750 cells mm^{-2}, with two images captured per trial after 24 h of culture.

significant differences between each cell type (Figure 8E, Table S3, Supporting Information). The similarities in cell phenotype response reflect the lack of incorporated bioactive components within the scaffolds. Any differences in alignment could only be attributed to differences in physical preference between each cell type. However, despite variability in characterization for each spin time, both Schwann cells and fibroblasts tended to respond with alignment on scaffolds. As additional cell responses are catalogued, it may arise that PVDF-TrFE fibers promote ubiquitous enhancement of PNS regenerative markers.

Scaffold biocompatibility was ensured through a multifaceted litmus test. First, it was established that DMF and acetone, two common organic solvents that are nonetheless toxic to a multitude of tissue, were relatively inert when abutted with biological structures.[72] Second, penetration, adherence, elongation, and alignment of both cells were either enhanced or otherwise undeterred relative to standard cultures and unaligned

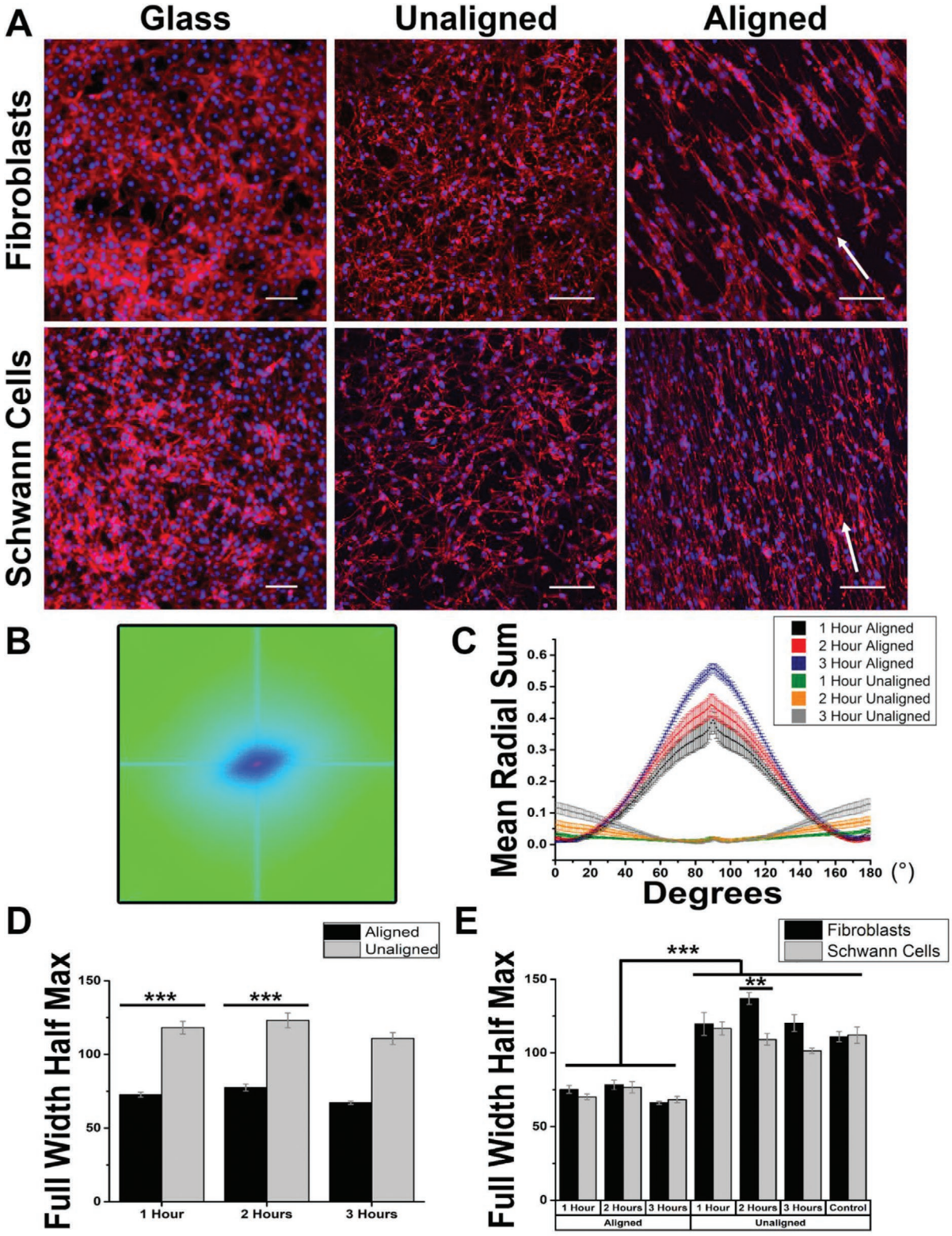

Figure 8. Aligned scaffolds promoted the alignment of both Schwann cells and fibroblasts. A) Representative confocal images showing cells seeded on glass coverslips alone, 1 h unaligned scaffolds, and 1 h aligned scaffolds. Scale bar = 100 µm. B) Representative spectrum of FFT of immunolabeled cell images. C) Mean radial sums generated from B) oval profiles and measured from 0° to 180°. D) Full width at half-maximum values calculated from C) radial sums curves for cells on aligned and unaligned scaffolds. E) Full width at half-maximum values for individual Schwann cells and fibroblasts on aligned and unaligned scaffolds. B–E) Cells imaged on scaffolds of 1, 2, and 3 h fabrication times, $n = 3$ unique trials per condition seeded at 750 cells mm^{-2}, with two images captured per trial after 24 h of culture. Data are reported as mean ± SEM. $^{*}p \leq 0.05$; $^{**}p \leq 0.005$; $^{***}p \leq 0.0005$.

fibrous scaffolds. Schwann cells and fibroblasts were utilized to emulate a regenerative PNS environment due to the interplay between the two cell types post-injury.[19,27,73,74] Schwann cells differentiate into a progenitor phenotype following traumatic injuries in order to secrete extracellular matrix proteins.[75] Fibroblasts, like Schwann cells, also play a critical role in PNS regeneration.[19,27,73,74,76–78] First, they are a primary source of fibronectin, an ECM protein crucial to the formation of Bands of Büngner.[76] Further, they help facilitate the sorting of Schwann cells during regeneration and promote the secretion of collagen, basal lamina, brain derived neurotrophic factor, and glial derived neurotrophic factor, post-injury.[19]

Our analysis simultaneously confirmed the biocompatibility of Schwann cells and fibroblasts while introducing unique characterization methods to assess phenotype response. Using adhesion as a marker for viability, penetration as a marker for in vivo applicability, and alignment as a marker for regenerative response, we have quantitatively detailed the biological response to changes in physical characteristics, crystalline structure, and piezoelectricity of PVDF-TrFE scaffolds. Though it will be challenging to further establish ideal thresholds for these measurable parameters, the cell-scaffold interactions observed suggest that PVDF-TrFE is a robust therapeutic material deserving of continued evaluation.

3. Conclusion

The use of piezoelectric, electrospun fibers in tissue engineering applications is a relatively new research area. Our work sought to determine the physical, chemical, and piezoelectric conditions necessary for a PVDF-TrFE scaffold to impart the appropriate cell phenotypic response for ultimate tissue engineering applications. Therefore, we performed an analysis of the piezoelectric potential of a scaffold developed using 20% (w/v) PVDF-TrFE in (6:4) DMF-Acetone solvent for fabrication of scaffolds over 1, 2, and 3 h of electrospinning. Scaffolds were further examined for biocompatibility using two separate PNS-relevant cells. Despite differences in composition and physical activity for different spin times, the scaffolds proved to be viable templates for cell growth, and emphatically capable of promoting quantifiable regenerative cell phenotype markers such as alignment of cells with the fibers and penetration into the scaffolds. Specifically, aligned 2 h spun scaffolds had sufficient porosity (greater than 70%), and were significantly stronger and more hydrophilic than other conditions. While the β phase configuration derived from FTIR and XRD spectra for 2 h spun scaffolds was slightly lower than 1 and 3 h scaffolds, the physical properties examined were found to be more variable between experimental conditions than β phase configuration. Finally, though 1 and 3 h aligned scaffolds exhibited a similar ability to direct cell behavior, and were both more adept at adhering cells after 24 h, it is believed that the favorable physical and electrical characterization of 2 h aligned scaffolds were more relevant toward controlling regenerative capabilities. Further analysis of PVDF-TrFE scaffolds is needed and should focus upon additional cell response cataloging as well as in vivo implementations, with an emphasis upon the relationship between piezoelectric output and tissue response at physiologically relevant levels. Ultimately, these scaffolds can be used as templates for broader tissue engineering applications in PNS regeneration and hold immense potential as multicue biomaterials.

4. Experimental Section

Electrospinning: PVDF-TrFE scaffolds were fabricated using an aligned electrospinning configuration (Fluidnatek LE-50).[54,79] Briefly, 20% (w/v) PVDF-TrFE (70/30) (PolyKTechnologies, State College, PA) was dissolved in a mixture of dimethylformamide and acetone (6:4), loaded into a syringe using a 20-gauge needle, and ejected at a flow rate of 1 mL h^{-1}. The collector was placed 10 cm from the needle tip, wrapped with a conductive polymer liner (McMaster-Carr), and rotated at 2000 rpm to create aligned fibers.[80] Unaligned fibers were fabricated by slowing the collector rotation to 200 rpm. A voltage (15 kV) was applied to the needle tip while the rotating collector was grounded. For both aligned and unaligned fibers, the polymer solution was spun for either 1, 2, or 3 h.

Fourier Transform Infrared Spectroscopy: Scaffolds were evaluated using Attenuated Total Reflectance (ATR) Fourier transform infrared spectroscopy (Nicolet 6700 FTIR with Smart Orbit diamond ATR). The range was set to 4000–400 cm^{-1} with a resolution of 4 cm^{-1}. FTIR results were used to quantify the percentage of piezoelectric β phase in the PVDF-TrFE sample. Calculation methods typically assumed that absorption spectra follow the Lambert-Beer Law.[55,81] The fraction of β phase content was thus estimated by

$$F(\beta) = \frac{A_\beta}{(K_\beta/K_\alpha)A_\alpha + A_\beta} \quad (1)$$

where $F(\beta)$ is the fraction of β-phase content in the sample, K_β and K_α are the absorption coefficients at 840 and 766 cm^{-1}, respectively (the values of which are 7.7×10^4 and 6.1×10^4 cm^2 mol^{-1}),[81] and A_β and A_α are the absorbance at 840 and 766 cm^{-1}, respectively.

X-Ray Diffraction: X-ray diffraction (X'Pert Pro Diffractometer) was used to evaluate the crystalline structure of the scaffolds. Samples were irradiated with monochromatic CuK_α with a scan rate of 0.013° s^{-1}, and 2θ was kept between 15° and 43°.

Piezoelectric Characterization: To demonstrate piezoelectricity of PVDF-TrFE microfibers, electrical response of the scaffold was qualitatively measured as the scaffold was bent into a parabolic shape by manually lifting a wire to an amplitude of ≈5 mm in height to exert pressure and placed down to release pressure. Two ends of a PVDF-TrFE scaffold were anchored to the glass slide with conductive silver paste (Ted Pella, INC.) to ensure probes maintained sufficient contact with scaffold.[82] The piezoelectric output was measured as the resulting current over time. Controls were performed by measuring the current across the configuration described with no external force applied. The experiments were run with a potential (5 V) applied onto the microfibers with a Hewlett-Packard 4140B pA Meter in a two-probe configuration. Additional controls were conducted by applying an equivalent amount of conductive silver paint to glass slides at an equivalent separated distance as the PVDF-TrFE experiment. An *I–V* sweep was conducted (1–16 V) and the current across each slide was analyzed.

Physical Characterization of PVDF: Fiber Morphology: Fiber morphology was characterized using scanning electron microscopy (ApreoC SEM, ThermoFisher). Two samples of each polymer concentration were prepared by sputter coating (Desk V, DentonVacuum) a layer of gold/palladium for 10 s on polymers. Five images per sample were taken with a 5 mm working distance and an acceleration voltage of 2 kV. Fiber diameter measurements were performed using ImageJ software (version 1.52p), as previously described.[57,83] SEM images were captured with an FEI XL-30 microscope (Low-Vac) using an EDAX elemental analysis detector.

The scaffold thickness with the collector liner was recorded using calipers both with and without the fibrous scaffold, using the difference between measurements as the corresponding polymer thickness.

Mechanical Characterization: Unaligned and aligned scaffolds of each electrospinning time were prepared into samples of 20 mm × 30 mm, placed in a tensile testing machine (Test Resources Universal Test Machine), and stretched at a rate of 1 mm min^{-1} while force and displacement were recorded to determine Young's modulus. Tensile testing was performed both parallel and perpendicular to the alignment of the fibers for aligned scaffolds and in a single direction for unaligned scaffolds.

Porosity: The porosity of scaffolds was estimated as previously outlined[57,82] for both unaligned and aligned fibrous scaffolds of 1, 2, and 3 h spin times. The density of a sample scaffold ($\rho_{scaffold}$) was calculated by measuring its dimensions and weighing the sample. The percentage of the porosity was then calculated using the following equation

$$\text{Porosity}\,(\%) = \left(1 - \frac{\rho_{scaffold}}{\rho_{raw}}\right) \times 100\% \quad (2)$$

where the density of the unprocessed PVDF-TrFE powder (ρ_{raw}) was 1.88 g cm^{-3}.

Contact Angle: The surface contact angle of the PVDF-TrFE microfibers at 23 °C was measured with a VCA Optima video-based contact angle meter (AST Products, INC).[54] A droplet of deionized water (3.0 ± 0.1 µL) was deposited onto the fiber sample and the contact angle was calculated manually using the VCA Optima software by placing five markers around the perimeter of the droplet. Experiments were repeated for five different locations on each scaffold for both unaligned and aligned polymers of 1, 2, and 3 h spin times. The average contact angle between each side of the droplet and the scaffold surface was then automatically calculated.

Cell culture: RT4-D6P2T Schwann cells (ATCC) and NIH 3T3 fibroblasts (ATCC) were cultured in high glucose Dulbecco's modified eagle medium (DMEM) (SH30022) (GE Healthcare) supplemented with either fetal bovine serum (10%) (Thermo Fisher) for Schwann cells or bovine calf serum (10%) (Thermo Fisher) for fibroblasts and pen/strep (1%) (Thermo Fisher) at 37 °C using CO_2 (5%) and 95% relative humidity. Cells were grown to subconfluence before passaging via phosphate buffered saline (PBS) (Thermo Fisher) wash and dissociation by trypsin (0.25%) in versine (Gibco) solution.

PVDF-TrFE scaffolds were cut into ≈2 cm × 2 cm segments, placed on 18 mm diameter microscope coverslips (Fisher), and added to a 12-well plate. Coverslips were sterilized overnight under UV-light. Prior to cell seeding, polytetrafluoroethylene (PTFE) O-rings (ID, 10.8 mm; OD, 11.78 mm) (Wilmad Labglass) were placed upon the PVDF-TrFE segments to ensure polymers remain submerged after seeding. The polymer segments were rinsed with ethanol (70%) and washed twice with PBS. Schwann cells and fibroblasts were then mixed with media and seeded at a final density of 75 000 cells cm^{-2}.

Immunofluorescence and Microscopy: R457 rabbit antifibronectin polyclonal antiserum was kindly donated by Jean Schwarzbauer from Princeton University. The *N*-terminal 70 kDa terminal of rat fibronectin was used to raise R457 antiserum.[84] Alexa Flour 488 goat antimouse secondary antibody (A11001), DAPI (4′,6-Diamidino-2-Phenylindole, Dihydrochloride) (D1306), laminin from mouse (23017015), and rhodamine-phalloidin (R415) were purchased from ThermoFisher.

Postculture, PVDF-TrFE scaffolds were washed twice with PBS and fixed in formaldehyde (3.7%) for 15 min. Samples were washed twice with PBS and lysed with Triton X-100 (0.5%) for 5 min at 4 °C followed by two additional PBS washes. Samples were incubated in a dilution of 1:100 R457 primary antibody at 37 °C for 30 min and subsequently incubated in rhodamine-phalloidin (10 µg mL^{-1}) and Alexa Fluor 488 goat antimouse secondary antibody (1 µg mL^{-1}) at 37 °C for 30 min. Samples were then incubated in DAPI staining solution (300×10^{-9} M) at 37 °C for 5 min and then attached to glass microscope slides with mounting medium (50% glycerol, 20×10^{-3} M Tris, 0.5% *N*-propyl gallate) and sealed with clear nail polish.

Wide-field images were captured with a Nikon Eclipse Ti2 inverted microscope and a Nikon DS-Qi2 camera using both fluorescent and phase microscopy. Confocal images were captured with a Nikon eclipse Ti inverted microscope on a Nikon AIR confocal using fluorescent microscopy.

Cell Alignment, Proliferation, Adhesion, and Penetration into Scaffolds: For all cell-scaffold interaction analysis, three coverslips were created for each experimental condition. Cell adhesion was determined by culturing cells in medium supplemented with and without serum. Control was established by treating the polymers with UV-Ozone for 7 min and applying a coating of laminin protein (10 µg mL^{-1}) for 1 h at 37 °C. Three coverslips were created for each experimental condition and 15 images per slide were captured using the DAPI channel in Nikon NIS Elements software.

For cell proliferation, Schwann cells and fibroblasts were seeded at a low density of 50 cells mm^{-2} on both 2 h spun unaligned and aligned scaffolds and cultured for 24, 48, and 72 h. Multiple experiments with three coverslips each were created for each experimental condition and 15 images per slide were captured using the DAPI channel in Nikon Elements software. For both the adhesion and proliferation assays, the "Object Count" feature of the Elements software was used to automatically calculate the total number of cells per image. Cells cultured for 72 h were additionally stained for rhodamine-phalloidin and captured as representative images.

To analyze alignment and penetration, cells were cultured for 24 h under standard conditions on 1, 2, and 3 h spun scaffolds before being fixed, immunolabeled, and imaged with either phase microscopy or confocal microscopy. Representative images of cell cultures on scaffolds were created by overlaying DAPI and TRITC channels. For confocal images, a Z-stack was performed across the height of the scaffold and visualized using a maximum intensity projection on NIS Elements. 3D projections were created and color-coded for corresponding depths to determine the penetration of cells throughout the scaffolds. Two random images from each coverslip were captured using Nikon NIS Elements software.

Cell alignment was calculated using rhodamine-phalloidin staining in the NIH ImageJ software (version 1.52p) of cells on aligned and unaligned scaffolds, where representative images were processed using a Fast Fourier Transformation and subsequent oval profiles were quantified for radial sums from 0° to 180°. Full width at half-maximum values were then calculated from each respective radial sums curve. Two randomized images from each of the three coverslips were captured using Nikon NIS Elements software.

Statistical Analysis: Data were reported as mean values ± standard error. Statistical analysis was performed on excel and Origin 9.1. One-way analysis of variance (ANOVA) and Tukey's post-hoc test were used for comparative analysis and statistical significance, delineated as *, $p \leq 0.05$, ** $p \leq 0.005$, and ***, $p \leq 0.0005$.

Supporting Information

Supporting Information is available from the Wiley Online Library or from the author.

Acknowledgements

The authors would like to thank Dr. Andrew J. Steckl and Dr. Jason C. Heikenfeld for supplying experimental devices and technical guidance, Eric Frantz and Daewoo Han for assistance in electrical characterization, Melodie Fickenscher for conducting SEM imaging, and Avani Kabra for preliminary research and electrospinning experimentation. The authors would also like to thank Dr. Matt Kofron and Evan Meyer at Cincinnati Children's Hospital for assistance with confocal microscopy.

Conflict of Interest

The authors declare no conflict of interest.

Keywords

cell adhesion, nanofiber scaffolds, piezoelectric biomaterials, Schwann cells, tissue engineering

Received: May 7, 2020
Revised: June 28, 2020
Published online:

[1] C. A. Taylor, D. Braza, J. B. Rice, T. Dillingham, *Am. J. Phys. Med. Rehabil.* **2008**, *87*, 381.
[2] H. Azhary, M. U. Farooq, M. Bhanushali, A. Majid, M. Y. Kassab, *Am. Fam. Physician* **2010**, *81*, 887.
[3] C. N. Martyn, R. A. C. Hughes, *J. Neurol., Neurosurg. Psychiatry* **1997**, *62*, 310.
[4] R. M. Menorca, T. S. Fussell, J. C. Elfar, *Hand Clinics* **2013**, *29*, 317.
[5] Q. Li, P. Zhang, X. Yin, N. Han, Y. Kou, B. Jiang, *J. Neurosurg.* **2014**, *121*, 415.
[6] E. O. Johnson, P. N. Soucacos, *Injury* **2008**, *39*, 30.
[7] M. F. Griffin, M. Malahias, S. Hindocha, W. S. Khan, *Open Orthop. J.* **2014**, *8*, 409.
[8] N. L. Nerurkar, S. Sen, B. M. Baker, D. M. Elliott, R. L. Mauck, *Acta Biomater.* **2011**, *7*, 485.
[9] C. D. McCaig, A. M. Rajnicek, B. Song, M. Zhao, *Trends Neurosci.* **2002**, *25*, 354.
[10] T. Courtney, M. S. Sacks, J. Stankus, J. Guan, W. R. Wagner, *Biomaterials* **2006**, *27*, 3631.
[11] L. Wang, Y. Wu, T. Hu, B. Guo, P. X. Ma, *Acta Biomater.* **2017**, *59*, 68.
[12] S. M. Damaraju, S. Wu, M. Jaffe, T. L. Arinzeh, *Biomed. Mater.* **2013**, *8*, 045007.
[13] Y. S. Lee, T. L. Arinzeh, *Tissue Eng., Part A* **2012**, *18*, 2063.
[14] Y. Wu, L. Wang, B. Guo, Y. Shao, P. X. Ma, *Biomaterials* **2016**, *87*, 18.
[15] Y. Wu, L. Wang, T. Hu, P. X. Ma, B. Guo, *J. Colloid Interface Sci.* **2018**, *518*, 252.
[16] S. Wu, M. S. Chen, P. Maurel, Y. S. Lee, M. B. Bunge, T. L. Arinzeh, *J. Neural. Eng.* **2018**, *15*, 056010.
[17] T. M. Dinis, R. Elia, G. Vidal, Q. Dermigny, C. Denoeud, D. L. Kaplan, C. Egles, F. Marin, *J. Mech. Behav. Biomed. Mater.* **2015**, *41*, 43.
[18] Y. S. Lee, S. Wu, T. L. Arinzeh, M. B. Bunge, *Biotechnol. Bioeng.* **2017**, *114*, 444.
[19] Y. Wang, D. Li, G. Wang, L. Chen, J. Chen, Z. Liu, Z. Zhang, H. Shen, Y. Jin, Z. Shen, *Int. J. Biol. Sci.* **2017**, *13*, 1507.
[20] M. Feughelman, D. Lyman, E. Menefee, B. Willis, *Int. J. Biol. Macromol.* **2003**, *33*, 149.
[21] E. Fukada, I. Yasuda, *Jpn. J. Appl. Phys.* **1964**, *3*, 117.
[22] E. Fukada, I. Yasuda, *J. Phys. Soc. Jpn.* **1957**, *12*, 1158.
[23] A. Hoke, R. Redett, H. Hameed, R. Jari, C. Zhou, Z. B. Li, J. W. Griffin, T. M. Brushart, *J. Neurosci.* **2006**, *26*, 9646.
[24] Z. Xu, J. A. Orkwis, B. M. DeVine, G. M. Harris, *J. Tissue Eng. Regener. Med.* **2019**, *14*, 229.
[25] J. A. Gomez-Sanchez, L. Carty, M. Iruarrizaga-Lejarreta, M. Palomo-Irigoyen, M. Varela-Rey, M. Griffith, J. Hantke, N. Macias-Camara, M. Azkargorta, I. Aurrekoetxea, V. G. De Juan, H. B. Jefferies, P. Aspichueta, F. Elortza, A. M. Aransay, M. L. Martinez-Chantar, F. Baas, J. M. Mato, R. Mirsky, A. Woodhoo, K. R. Jessen, *J. Cell Biol.* **2015**, *210*, 153.
[26] J. A. Gomez-Sanchez, K. S. Pilch, M. van der Lans, S. V. Fazal, C. Benito, L. J. Wagstaff, R. Mirsky, K. R. Jessen, *J. Neurosci.* **2017**, *37*, 9086.
[27] K. R. Jessen, R. Mirsky, A. C. Lloyd, *Cold Spring Harbor Perspect. Biol.* **2015**, *7*, a020487.
[28] Y. Li, C. Liao, S. C. Tjong, *Nanomaterials* **2019**, *9*, 952.
[29] G. Ico, A. Showalter, W. Bosze, S. C. Gott, B. S. Kim, M. P. Rao, N. V. Myung, J. Nam, *J. Mater. Chem. A* **2016**, *4*, 2293.
[30] C. A. Bashur, L. A. Dahlgren, A. S. Goldstein, *Biomaterials* **2006**, *27*, 5681.
[31] G. T. Christopherson, H. Song, H. Q. Mao, *Biomaterials* **2009**, *30*, 556.
[32] S. Ramakrishna, K. Fujihara, W.-E. Teo, T. Yong, Z. Ma, R. Ramaseshan, *Mater. Today* **2006**, *9*, 40.
[33] P. P. Provenzano, D. R. Inman, K. W. Eliceiri, S. M. Trier, P. J. Keely, *Biophys. J.* **2008**, *95*, 5374.
[34] L. Ghasemi-Mobarakeh, M. Morshed, K. Karbalaie, M. A. Fesharaki, M. Nematallahi, M. H. Nasr-Esfahani, H. Baharvand, *Int. J. Artif. Organs* **2009**, *32*, 150.
[35] M. P. Prabhakaran, J. Venugopal, C. K. Chan, S. Ramakrishna, *Nanotechnology* **2008**, *19*, 455102.
[36] D. Liang, B. S. Hsiao, B. Chu, *Adv. Drug Delivery Rev.* **2007**, *59*, 1392.
[37] X. Zhu, W. Cui, X. Li, Y. Jin, *Biomacromolecules* **2008**, *9*, 1795.
[38] M. N. Sarip, R. Mohd Dahan, Y. S. Ling, M. H. M. Wahid, A. N. Arshad, D. Kamarun, *Adv. Mater. Res.* **2014**, *895*, 138.
[39] J. W. Chen, K. Lim, S. B. Bandini, G. M. Harris, J. A. Spechler, C. B. Arnold, R. Fardel, J. E. Schwarzbauer, J. Schwartz, *ACS Appl. Mater. Interfaces* **2019**, *11*, 15411.
[40] M. Baniasadi, Z. Xu, J. Cai, S. Daryadel, M. Quevedo-Lopez, M. Naraghi, M. Minary-Jolandan, *Polymer* **2017**, *127*, 192.
[41] E. B. Evans, S. W. Brady, A. Tripathi, D. Hoffman-Kim, *Biomater. Res.* **2018**, *22*, 14.
[42] U. Stachewicz, R. J. Bailey, W. Wang, A. H. Barber, *Polymer* **2012**, *53*, 5132.
[43] N. J. Amoroso, A. D'Amore, Y. Hong, C. P. Rivera, M. S. Sacks, W. R. Wagner, *Acta Biomater.* **2012**, *8*, 4268.
[44] J. Nam, J. Johnson, J. J. Lannutti, S. Agarwal, *Acta Biomater.* **2011**, *7*, 1516.
[45] G. M. Harris, M. E. Piroli, E. Jabbarzadeh, *Adv. Funct. Mater.* **2014**, *24*, 2396.
[46] G. M. Harris, T. Shazly, E. Jabbarzadeh, *PLoS One* **2013**, *8*, e81113.
[47] A. J. Engler, S. Sen, H. L. Sweeney, D. E. Discher, *Cell* **2006**, *126*, 677.
[48] J. P. Fu, Y. K. Wang, M. T. Yang, R. A. Desai, X. A. Yu, Z. J. Liu, C. S. Chen, *Nat. Methods* **2010**, *7*, 733.
[49] C. Bonnans, J. Chou, Z. Werb, *Nat. Rev. Mol. Cell Biol.* **2014**, *15*, 786.
[50] T. Yeung, P. C. Georges, L. A. Flanagan, B. Marg, M. Ortiz, M. Funaki, N. Zahir, W. Ming, V. Weaver, P. A. Janmey, *Cell Motil. Cytoskeleton* **2005**, *60*, 24.
[51] A. P. Balgude, X. Yu, A. Szymanski, R. V. Bellamkonda, *Biomaterials* **2001**, *22*, 1077.
[52] A. J. Man, H. E. Davis, A. Itoh, J. K. Leach, P. Bannerman, *Tissue Eng., Part A* **2011**, *17*, 2931.
[53] C. M. Wu, M. H. Chou, *Compos. Sci. Technol.* **2016**, *127*, 127.
[54] H. G. Jeong, Y. S. Han, K. H. Jung, Y. J. Kim, *Nanomaterials* **2019**, *9*, 184.
[55] P. Martins, A. C. Lopes, S. Lanceros-Mendez, *Prog. Polym. Sci.* **2014**, *39*, 683.
[56] Z.-Y. Wang, H.-Q. Fan, K.-H. Su, Z.-Y. Wen, *Polymer* **2006**, *47*, 7988.
[57] Y.-S. Lee, T. Livingston Arinzeh, *Polymers* **2011**, *3*, 413.
[58] L. Persano, C. Dagdeviren, Y. Su, Y. Zhang, S. Girardo, D. Pisignano, Y. Huang, J. A. Rogers, *Nat. Commun.* **2013**, *4*, 1633.
[59] M. Hoop, X. Z. Chen, A. Ferrari, F. Mushtaq, G. Ghazaryan, T. Tervoort, D. Poulikakos, B. Nelson, S. Pane, *Sci. Rep.* **2017**, *7*, 4028.
[60] S. Y. Chew, R. Mi, A. Hoke, K. W. Leong, *Biomaterials* **2008**, *29*, 653.
[61] A. N. Koppes, N. W. Zaccor, C. J. Rivet, L. A. Williams, J. M. Piselli, R. J. Gilbert, D. M. Thompson, *J. Neural. Eng.* **2014**, *11*, 046002.
[62] S. L. Rogers, K. J. Edson, P. C. Letourneau, S. C. McLoon, *Dev. Biol.* **1986**, *113*, 429.
[63] M. L. Feltri, L. Wrabetz, *J. Peripher. Nerv. Syst.* **2005**, *10*, 128.
[64] J. R. Couchman, M. Höök, D. A. Rees, R. Timpl, *J. Cell Biol.* **1983**, *96*, 177.

[65] R. P. Mecham, *FASEB J.* **1991**, *5*, 2538.
[66] N. R. Smalheiser, N. B. Schwartz, *Cell Biol.* **1987**, *84*, 6457.
[67] P. Hitscherich, S. Wu, R. Gordan, L. H. Xie, T. Arinzeh, E. J. Lee, *Biotechnol. Bioeng.* **2016**, *113*, 1577.
[68] A. Wang, Z. Liu, M. Hu, C. Wang, X. Zhang, B. Shi, Y. Fan, Y. Cui, Z. Li, K. Ren, *Nano Energy* **2018**, *43*, 63.
[69] J. He, Y. Liang, M. Shi, B. Guo, *Chem. Eng. J.* **2020**, *385*, 123464.
[70] L. Wang, Y. Wu, T. Hu, P. X. Ma, B. Guo, *Acta Biomater.* **2019**, *96*, 175.
[71] G. M. Harris, N. N. Madigan, K. Z. Lancaster, L. W. Enquist, A. J. Windebank, J. Schwartz, J. E. Schwarzbauer, *Matrix Biol.* **2017**, *60–61*, 176.
[72] F. Armutcu, Ö. Coskun, A. Gürel, S. Sahin, M. Kanter, A. Cihan, K. V. Numanoglu, C. Altinyazar, *Cell Biol. Toxicol.* **2005**, *21*, 53.
[73] K. R. Jessen, R. Mirsky, *J. Physiol.* **2016**, *594*, 3521.
[74] M. P. Clements, E. Byrne, L. F. Camarillo Guerrero, A. L. Cattin, L. Zakka, A. Ashraf, J. J. Burden, S. Khadayate, A. C. Lloyd, S. Marguerat, S. Parrinello, *Neuron* **2017**, *96*, 98.
[75] T. H. Barker, *Biomaterials* **2011**, *32*, 4211.
[76] L. Dreesmann, U. Mittnacht, M. Lietz, B. Schlosshauer, *Eur. J. Cell Biol.* **2009**, *88*, 285.
[77] V. J. Obremski, P. M. Wood, M. B. Bunge, *Dev. Biol.* **1993**, *160*, 119.
[78] S. Parrinello, I. Napoli, S. Ribeiro, P. Wingfield Digby, M. Fedorova, D. B. Parkinson, R. D. Doddrell, M. Nakayama, R. H. Adams, A. C. Lloyd, *Cell* **2010**, *143*, 145.
[79] L. Huang, J. T. Arena, J. R. McCutcheon, *J. Membr. Sci.* **2016**, *499*, 352.
[80] L. C. Lins, F. Wianny, S. Livi, C. Dehay, J. Duchet-Rumeau, J. F. Gerard, *J. Biomed. Mater. Res., Part B* **2017**, *105*, 2376.
[81] V. Sencadas, M. V. Moreira, S. Lanceros-Méndez, A. S. Pouzada, R. Gregório Filho, *Mater. Sci. Forum* **2006**, *514–516*, 872.
[82] J. Joseph, M. Kumar, S. Tripathy, G. D. V. S. Kumar, S. G. Singh, S. R. K. Vanjari, in *2018 IEEE Sensors*, Institute of Electrical and Electronics Engineers, New Delhi, India **2018**.
[83] K. Yu Wang, T.-S. Chung, M. Gryta, *Chem. Eng. Sci.* **2008**, *63*, 2587.
[84] K. M. Aguirre, R. J. McCormick, J. E. Schwarzbauers, *J. Biol. Chem.* **1994**, *269*, 27863.

Supporting Information

for *Macromol. Biosci.,* DOI: 10.1002/mabi.202000197

Development of a Piezoelectric PVDF-TrFE Fibrous Scaffold to Guide Cell Adhesion, Proliferation, and Alignment

Jacob A. Orkwis, Ann K. Wolf, Syed M. Shahid, Corinne Smith, Leyla Esfandiari,* and Greg M. Harris*

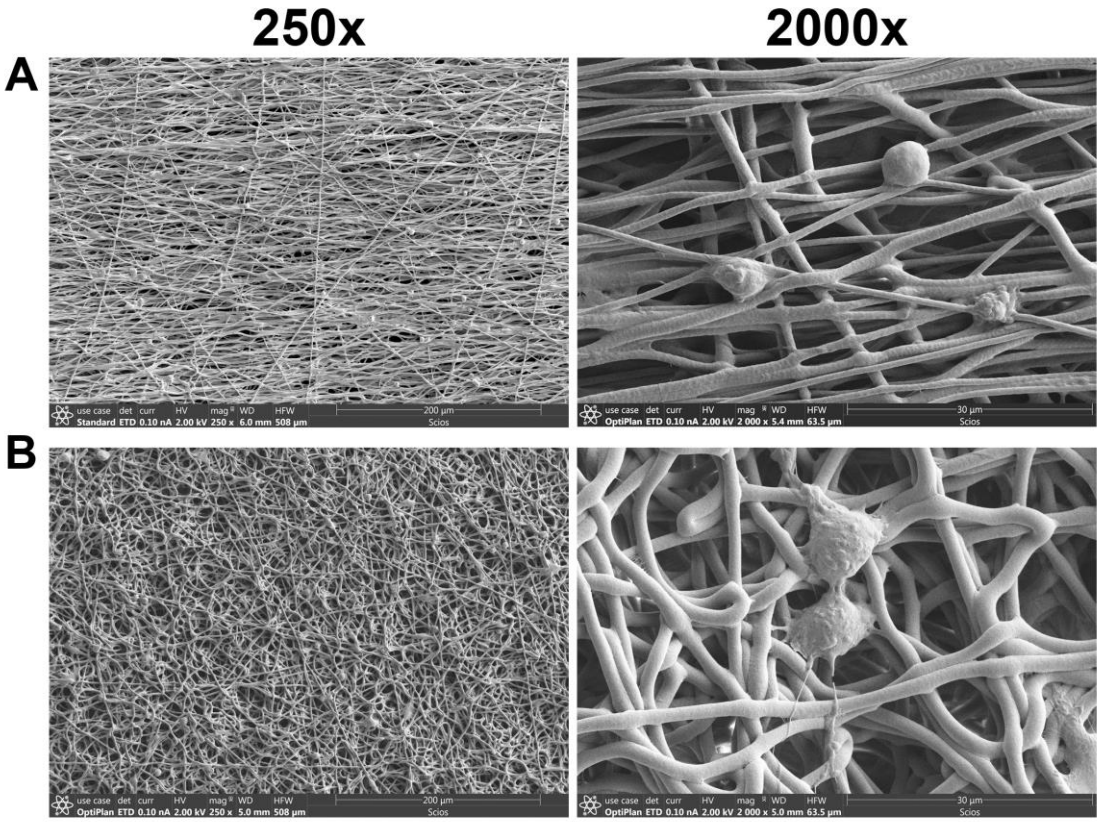

Figure S1. Representative SEM images of (A) aligned and (B) unaligned PVDF-TrFE scaffolds seeded with 750 cells mm^{-2} and cultured for 24 hours at 250x (left) and 2000x (right) magnification.

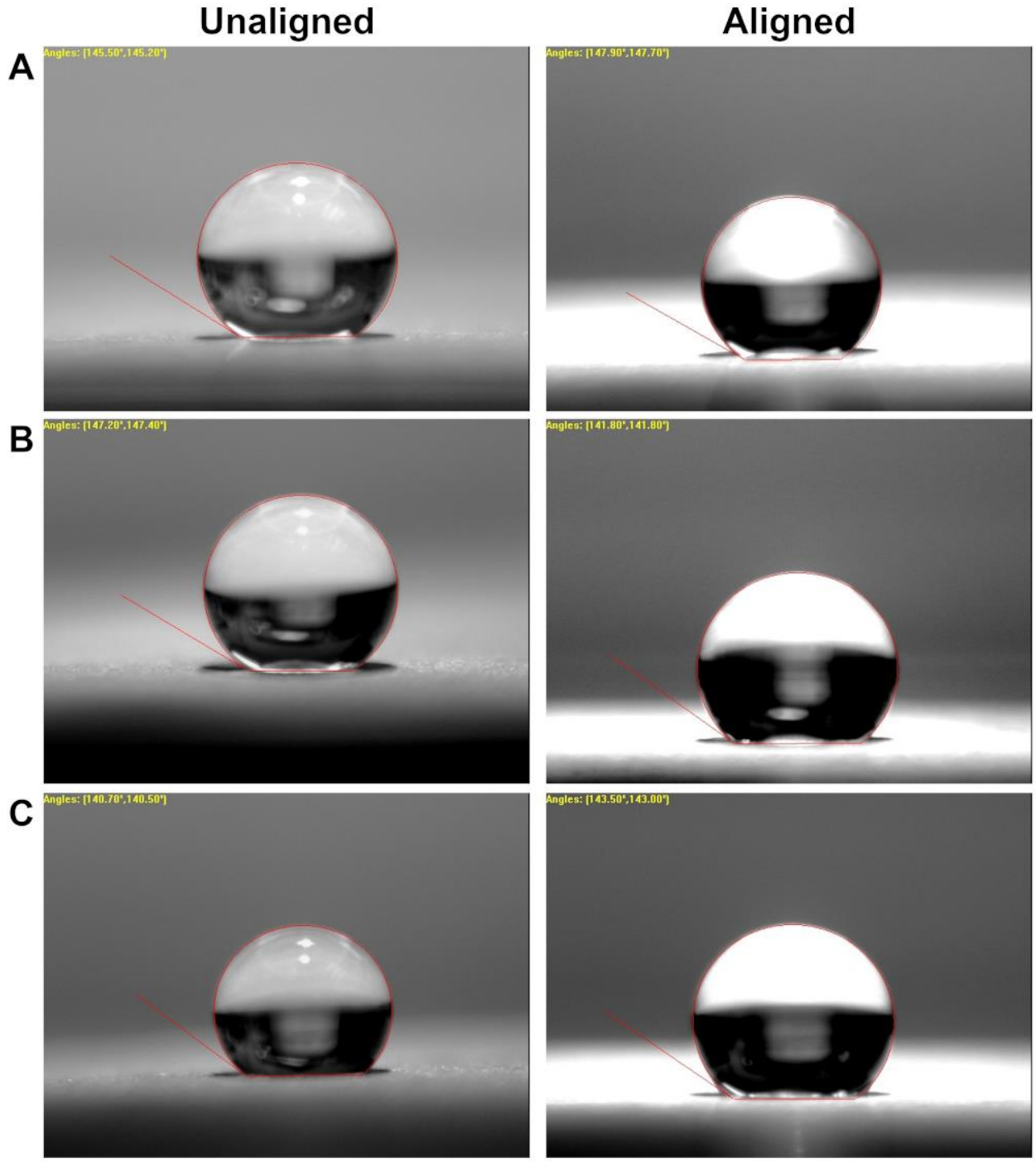

Figure S2. Representative water contact angle images for both unaligned (left) and aligned (right) PVDF-TrFE scaffolds of (A) 1, (B) 2, and (C) 3 hour fabrication times. Mean contact angles of all trials for unaligned scaffolds were (A) 145.35°, (B) 147.30°, (C) 140.60° and (A) 147.80°, (B) 141.80°, (C) 143.25° for aligned scaffolds.

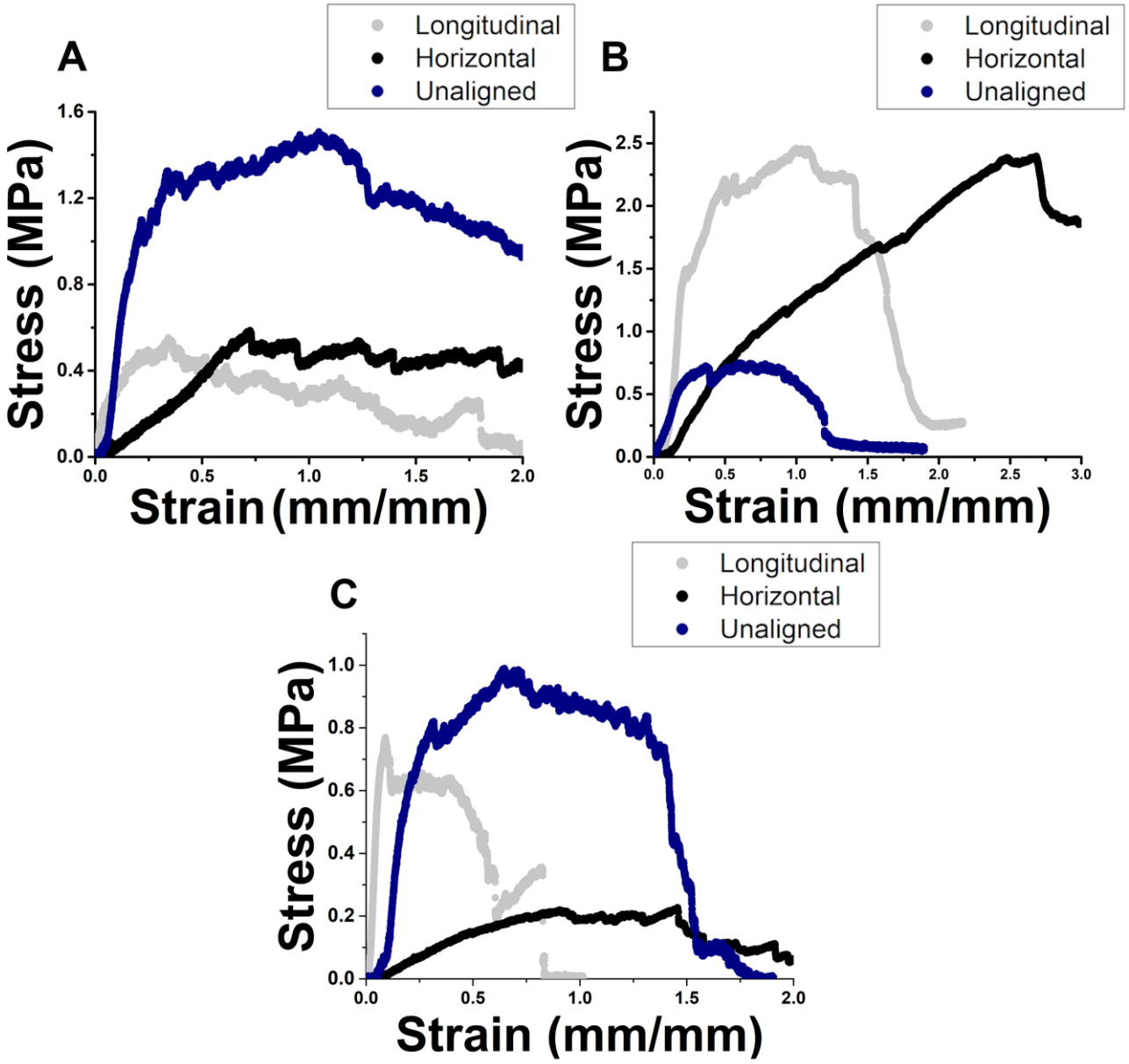

Figure S3. Representative stress-strain curves generated by one unique PVDF-TrFE sample of 1 (A), 2 (B), and 3 (C) hour fabrication times.

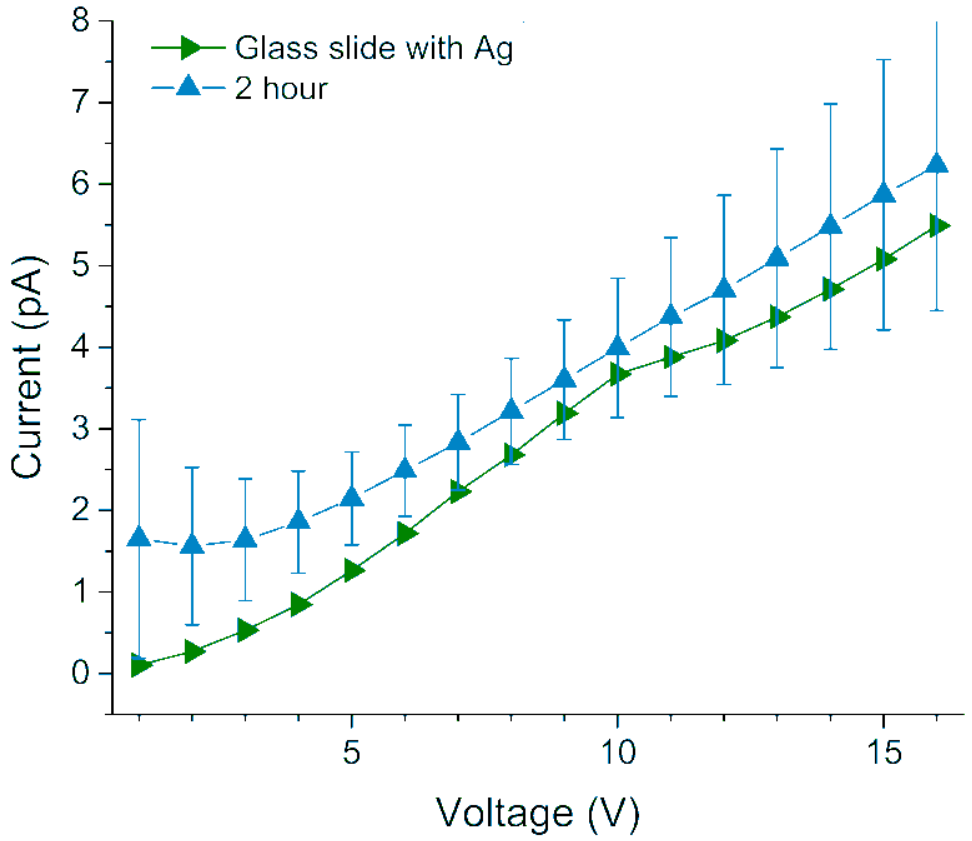

Figure S4. Current (I) plotted against Voltage (V) for PVDF-TrFE scaffold fabricated for 2 hours without an applied mechanical force. Data are reported as mean ± SEM

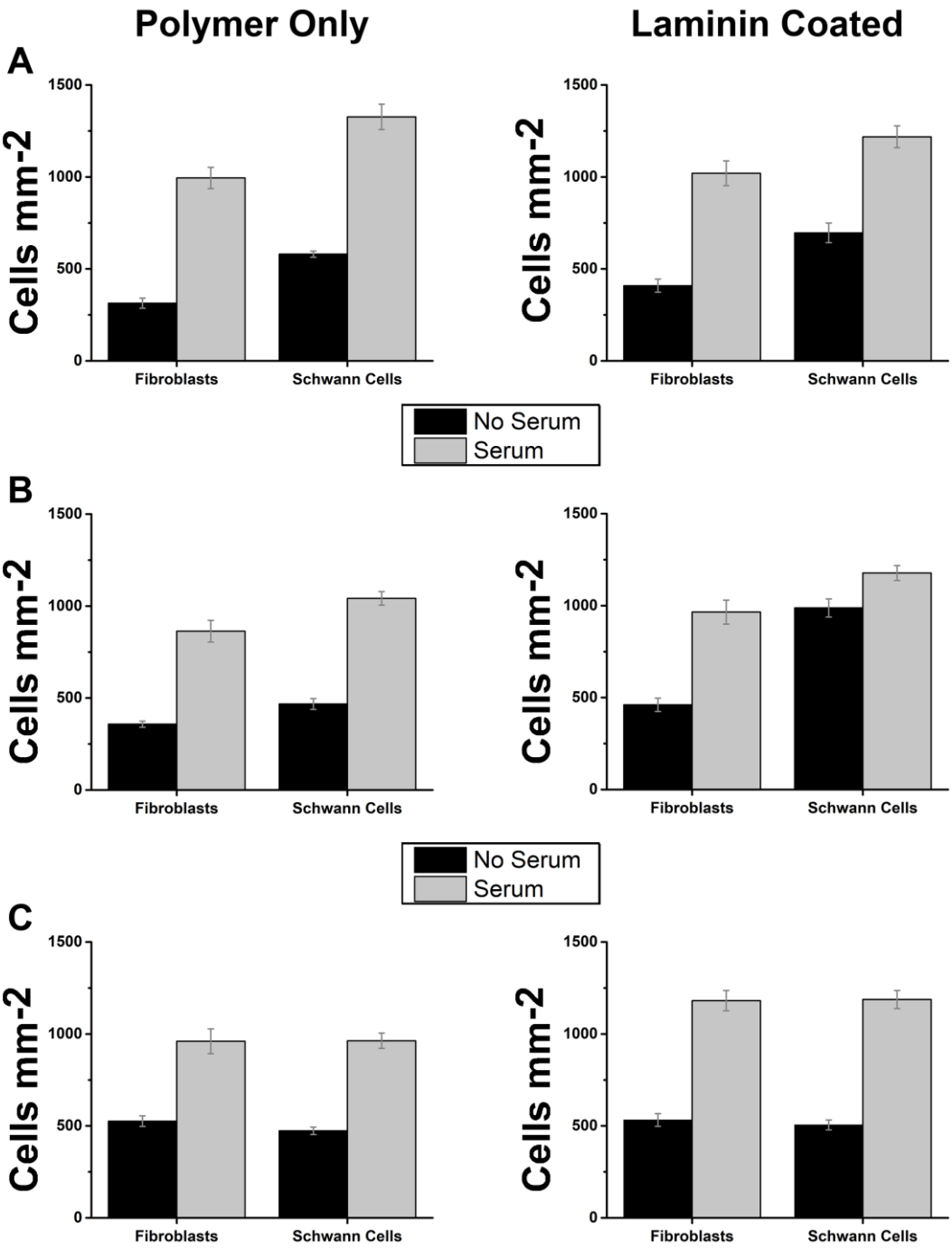

Figure S5. Total cells per area on (A) 1, (B) 2, and (C) 3 hour electrospun scaffolds coated without (left) or with (right) laminin protein and with or without serum. Data are reported as mean ± SEM. *$p \leq 0.05$, **$p \leq 0.005$, ***$p \leq 0.0005$.

Table S1. P-Values for Tukey's post-hoc tests on (A) mean porosity values, (B) mean thickness values, (C) mean water contact angles, and (D) mean Young's Moduli tested both longitudinally, horizontally, and unaligned relative to fiber alignment. (A-D) For 1, 2, and 3 hour spun scaffolds. Gray-shaded boxes indicate significance., where *$p \leq 0.05$, **$p \leq 0.005$, ***$p \leq 0.0005$.

A

		1 Hour		2 Hours		3 Hours	
		Aligned	Unaligned	Aligned	Unaligned	Aligned	Unaligned
1 Hour	Aligned	-	0.2769	0.9968	0.1930	0.8919	1.43E-08***
	Unaligned	-	-	0.04862*	0.9999	0.01261*	1.79E-08***
2 Hours	Aligned	-	-	-	0.02773*	0.9801	2.66E-08***
	Unaligned	-	-	-	-	0.006990*	1.73E-08***
3 Hours	Aligned	-	-	-	-	0.01261*	1.38E-08***
	Unaligned	-	-	-	-	-	-

B

		1 Hour		2 Hours		3 Hours	
		Aligned	Unaligned	Aligned	Unaligned	Aligned	Unaligned
1 Hour	Aligned	-	0.72231	6.56E-04**	0.61034	5.57E-08***	0.00189**
	Unaligned	-	-	0.11254	0.99998	3.21E-07***	0.10392
2 Hours	Aligned	-	-	-	0.15915	4.13E-06***	0.99676
	Unaligned	-	-	-	-	4.32E-07***	0.14098
3 Hours	Aligned	-	-	-	-	-	2.19E-04***
	Unaligned	-	-	-	-	-	-

C

		1 Hour		2 Hours		3 Hours	
		Aligned	Unaligned	Aligned	Unaligned	Aligned	Unaligned
1 Hour	Aligned	-	0.02614	1.30E-07***	0.82238	9.95E-05***	4.46E-08***
	Unaligned	-	-	5.96E-04**	0.00128**	0.26533	4.14E-07***
2 Hours	Aligned	-	-	-	4.73E-08***	0.16433	0.0155*
	Unaligned	-	-	-	-	4.54E-06	4.07E-08***
3 Hours	Aligned	-	-	-	-	-	8.85E-05***
	Unaligned	-	-	-	-	-	-

D

		1 Hour			2 Hours			3 Hours		
		Longitudinal	Horizontal	Unaligned	Longitudinal	Horizontal	Unaligned	Longitudinal	Horizontal	Unaligned
1 Hour	Longitudinal	-	0.9965	0.8756	0.00211*	1	0.9999	0.1460	0.9975	0.9999
	Horizontal	-	-	0.4513	4.42E-04***	0.9998	1	0.03417*	1	0.9276
	Unaligned	-	-	-	0.03908*	0.7527	0.6322	0.8381	0.4715	0.9888
2 Hours	Longitudinal	-	-	-	-	0.00125**	8.19E-04**	0.4900	4.74E-04***	0.006*
	Horizontal	-	-	-	-	-	1	0.09206	0.9999	0.9968
	Unaligned	-	-	-	-	-	-	0.06221	1	0.9847
3 Hours	Longitudinal	-	-	-	-	-	-	-	0.03668*	0.3278
	Horizontal	-	-	-	-	-	-	-	-	0.9374
	Unaligned	-	-	-	-	-	-	-		-

Table S2. P-Values for Tukey's post-hoc tests for adhesion of both Schwann cells and fibroblasts seeded on 1, 2, and 3 hour spun scaffolds with either laminin or no laminin coating and either serum or no serum supplemented in the growth medium. Gray-shaded boxes indicate significance, where *$p \leq 0.05$, **$p \leq 0.005$, ***$p \leq 0.0005$.

			1 Hour				2 Hours				3 Hours			
			Polymer Only		Laminin Coating		Polymer Only		Laminin Coating		Polymer Only		Laminin Coating	
			No Serum	Serum	No Serum	Serum	No Serum	Serum	No Serum	Serum	No Serum	Serum	No Serum	Serum
1 Hour	Polymer Only	No Serum	-	0***	0.5981	1.76E-09***	0.9999	2.66E-09***	1.72E-06***	0***	0.9959	2.21E-09***	0.9512	0***
		Serum	-	-	0***	0.9996	0***	0.00168**	6.30768E-09***	0.8130	0***	0.00357**	0***	1
	Laminin Coating	No Serum	-	-	-	0***	0.1720	8.40E-09***	0.02657*	2.03E-09***	0.9959	7.86E-09***	1	0***
		Serum	-	-	-	-	1.94E-09	0.03737*	8.71E-09***	0.9982	0***	0.0655	0***	0.9773
2 Hours	Polymer Only	No Serum	-	-	-	-	-	9.85E-10***	4.46E-08***	0***	0.8415	5.63E-10***	0.5893	0***
		Serum	-	-	-	-	-	-	0.000273553***	0.4098	5.39E-09***	1	6.46E-09***	0.0002003***
	Laminin Coating	No Serum	-	-	-	-	-	-	-	1.30E-08***	0.0004***	0.00011493***	0.0021**	5.01E-09***
		Serum	-	-	-	-	-	-	-	-	0***	0.5410	4.12E-10***	0.4863
3 Hours	Polymer Only	No Serum	-	-	-	-	-	-	-	-	-	4.90702E-09	1	1.38E-09***
		Serum	-	-	-	-	-	-	-	-	-	-	5.96E-09***	0.0004664***
	Laminin Coating	No Serum	-	-	-	-	-	-	-	-	-	-	-	0***
		Serum	-	-	-	-	-	-	-	-	-	-	-	-

Table S3. P-Values for Tukey's post-hoc tests for alignment quantifications of both Schwann cells and fibroblasts seeded on 1, 2, and 3 hour spun. Gray-shaded boxes indicate significance, where *$p \leq 0.05$, **$p \leq 0.005$, ***$p \leq 0.0005$.

		1 Hour		2 Hours		3 Hours	
		Aligned	Unaligned	Aligned	Unaligned	Aligned	Unaligned
1 Hour	Aligned	-	3.74E-08***	0.91616	0***	0.87086	2.55E-08***
	Unaligned	-	-	2.16E-08***	0.91039	0***	0.6541
2 Hours	Aligned	-	-	-	3.73E-08***	0.2891	3.45E-08***
	Unaligned	-	-	-	-	0***	0.12872
3 Hours	Aligned	-	-	-	-	-	3.92E-08***
	Unaligned	-	-	-	-	-	-